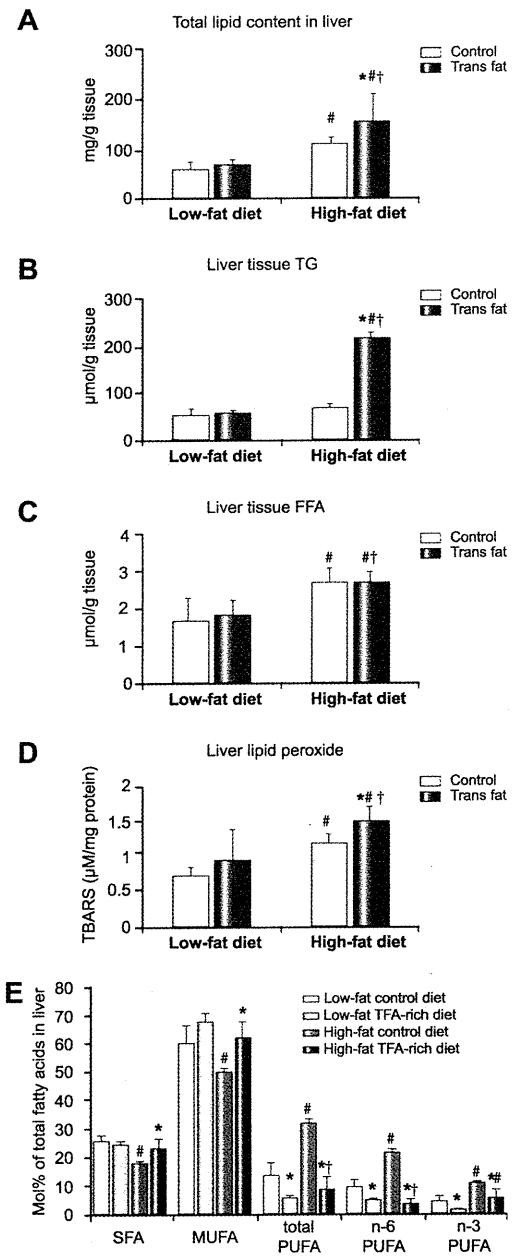

Fig. 2. Lipid accumulation in the liver. (A) Total lipid, (B) TG, and (C) FFA in the liver were measured and normalized to the tissue weight. (D) Lipid peroxide in the liver was measured and normalized by each amount of protein. (E) The hepatic fatty acid composition analyzed by gas chromatography was organized as follows: SFA, saturated fatty acid; MUFA, *cis*-monounsaturated fatty acid; PUFA, polyunsaturated fatty acid; *n*-6, *n*-6 PUFA; and *n*-3, *n*-3 PUFA ($n = 6$ for each group). *Significantly different from the control group with the same dietary composition; #significantly different from the low-fat diet with same dietary oil; † significantly different from LF-C-fed and HF-T-fed group.

terms of linoleic acid (18:2*n*-6), the precursor of arachidonic acid. Except for elaidic acid and arachidonic acid, there were no specific alterations for the HF-T group.

Cytokine-, adipokine- and lipid metabolism-related gene expression in liver

Real-time RCR showed that TNFα and inducible nitric oxide synthase (iNOS) mRNA expression increased in the HF groups compared to the LF groups by approximately 2-fold when evaluated for each C or T group (Table 4), while no difference was seen in IL-6 and transforming growth factor-β (TGF-β) mRNA expression in liver among all groups. In addition, adiponectin receptor 1 and 2 gene expression was measured as adipokine related genes, but they did not differ among all groups.

To examine the potential mechanisms of hepatic steatosis by the TFA-rich diet, we determined the expression of known mediators of lipogenesis, fatty acid oxidation and TG excretion in liver, the imbalance of which is thought to lead to steatosis. Sterol regulatory element-binding protein-1 (SREBP-1) induces fatty acid synthase (FAS) and acetyl CoA carboxylase (ACC), and is implicated in steatosis [27]. In relation to hepatic fatty acid synthesis, the mRNA expression of SREBP-1 was significantly elevated in the LF-T, HF-C and HF-T groups when compared to the LF-C group, whereas FAS and ACC were elevated significantly only in the HF-T group (Table 4). Peroxisome proliferator activated receptor γ (PPARγ) is also implicated in steatosis [33]. The expression of PPARγ1 did not differ among the groups, while PPARγ2 was significantly elevated 13-fold in the HF-C group and, remarkably, 50-fold in the HF-T group. Although, the expression of PPARγ coactivator-1β (PGC-1β), known to coactivate the SREBP-1 and stimulate lipogenic gene expression [19], was decreased in HF-fed mouse livers. The fatty acid oxidation-related genes of PPARα and carnitine palmitoyl transferase-1, and the TG excretion-related genes of microsomal triglyceride transfer protein and apolipoprotein B did not differ among the groups; fatty acid oxidation-related genes showed a tendency to be decreased in the LF-T group, but without statistical significance.

Concerning cholesterol metabolism-related gene expression in liver, SREBP-2 was increased in the HF groups, but was not affected by the dietary lipid sources. Hydroxymethylglutaryl-CoA synthase-1 and reductase were significantly increased and apolipoprotein A-1, a component of HDL, was decreased only in the HF-T group, while they did not change in the LF-T group, which showed an alteration of plasma cholesterol fraction (Table 4).

Phosphorylation status of AKT in high-fat diet-fed mice livers

As Koppe et al. suggested that TFA feeding increased insulin resistance in mice [17], and to determine if the exacerbating effects of TFA intake on liver were associated with increased insulin resistance, we evaluated the hepatic phosphorylation status of AKT (Fig. 3A). The phospho-AKT(Thr308) level was significantly decreased (Fig. 3B) and the phospho-AKT(Ser473) level was also decreased, but without statistical significance (Fig. 3C) as determined by densitometrical analysis.

TFA increases TNFα production and alters phagocytotic ability of KCs

The *cis*- or *trans*-fatty acid-containing medium showed no cytotoxicity towards KCs when compared to the fatty acid-free control medium (Fig. 4A). TNFα production of KCs induced by LPS was increased in both the C18:1 and C18:2 TFA-containing medium compared to that of *cis*-structural isomer-containing

Please cite this article in press as: Obara N et al. Possible involvement and the mechanisms of excess *trans*-fatty acid consumption in severe NAFLD in mice. J Hepatol (2010), doi:10.1016/j.jhep.2010.02.029

Research Article

Table 3. Individual fatty acid composition of the liver.

		Low-fat diet		High-fat diet	
		Control oil (LF-C)	TFA-rich oil (LF-T)	Control oil (HF-C)	TFA-rich oil (HF-T)
SFA					
Myristic	14:0	0.6 ± 0.1	0.5 ± 0.0	0.3 ± 0.1[‡]	0.4 ± 0.1[*†]
Palmitic	16:0	21.0 ± 1.6	19.2 ± 1.1	12.1 ± 0.6[‡]	18.7 ± 3.6[*]
Stearic	18:0	3.7 ± 0.8	3.6 ± 0.6	4.6 ± 0.6	3.3 ± 1.2
Arachidic	20:0	0.6 ± 0.3	1.0 ± 0.1[*]	0.6 ± 0.3	0.9 ± 0.3
MUFA					
Palmitoleic	16:1 *n*-7	6.9 ± 4.9	7.9 ± 4.8	2.5 ± 0.2	4.9 ± 1.0
Oleic	18:1	53.4 ± 6.7	59.8 ± 2.3	47.4 ± 1.3	57.2 ± 4.8[*‡†]
Elaidic	18:1 (9-*trans*)	0.0 ± 0.0	2.2 ± 0.5[*]	0.3 ± 0.2	6.2 ± 2.4[*‡†]
PUFA					
Linoleic	18:2 *n*-6	6.5 ± 2.1	2.1 ± 0.4[*]	18.1 ± 1.6[‡]	2.6 ± 1.4[*†]
α-Linolenic	18:3 *n*-3	0.6 ± 0.4	0.0 ± 0.0[*]	3.2 ± 0.5[‡]	0.2 ± 0.2[*]
Dihomo-γ-linolenic	20:3 *n*-6	0.2 ± 0.1	0.2 ± 0.1	0.5 ± 0.2[‡]	0.2 ± 0.2
Arachidonic	20:4 *n*-6	2.5 ± 0.9	2.2 ± 0.5	2.6 ± 0.6	0.6 ± 0.3[*‡†]
Eicosapentaenoic	20:5 *n*-3	0.4 ± 0.2	0.1 ± 0.0	1.4 ± 0.1[‡]	1.2 ± 0.9[‡†]
Docosapentaenoic	22:5 *n*-3	0.2 ± 0.1	0.0 ± 0.0	0.8 ± 0.0[‡]	0.4 ± 0.3[*‡†]
Docosahexaenoic	22:6 *n*-3	3.0 ± 1.1	1.0 ± 0.3	5.2 ± 0.4	3.2 ± 2.4

The relative percentage (mean ± SD) of each fatty acid to the total fatty acids is presented ($n = 6$ per each group).
[*] Significantly different from the corresponding control group with the same dietary composition; $p < 0.05$.
[‡] Significantly different from the low-fat diet with the same dietary lipid as a source; $p < 0.05$.
[†] Significantly different from low-fat control diet group; $p < 0.05$.

medium (Fig. 4B). However, IL-6 production by KCs did not differ between *cis*- and *trans*-fatty acid-containing medium for both C18:1 and C18:2, respectively (Fig. 4C). The phagocytotic ability of KCs incubated in *trans*-C18:1-containing medium was lower than that in *cis*-C18:1-containing medium (Fig. 4D), while the influence of the structural difference of C18:2 fatty acid was small (Fig. 4E).

Discussion

Both of the dietary lipid species [3] and their amounts [6,23] are known to affect hepatic steatosis and inflammation. TFAs have been mainly linked with coronary heart disease, possibly by decreasing HDL-cholesterol and increasing LDL-cholesterol [20,29]; while little attention has been paid to liver disease, even

Table 4. Cytokine-, adipokine- and lipid metabolism-related gene expression in liver.

		Low-fat TFA-rich (LF-T)	High-fat control (HF-C)	High-fat TFA-rich (HF-T)
Cytokine and adipokine				
Tumor necrosis factor	TNF	0.98 ± 0.20	2.11 ± 0.73[‡]	1.94 ± 0.77[‡†]
Interleukin-6	IL-6	1.30 ± 0.28	1.16 ± 0.14	1.10 ± 0.25
Transforming growth factor-β	TGB-β	0.86 ± 0.17	1.35 ± 0.50	0.98 ± 0.22
Nitric oxide synthase 2, inducible	iNOS	1.29 ± 0.34	2.23 ± 0.75[‡]	2.69 ± 0.74[‡†]
Adiponectin receptor 1	AdipoR1	1.01 ± 0.17	1.29 ± 0.29	1.21 ± 0.25
Adiponectin receptor 2	AdipoR2	0.92 ± 0.16	1.20 ± 0.22	1.28 ± 0.26
Lipogenesis				
Fatty acid synthase	FAS	1.36 ± 0.21	0.79 ± 0.12	1.69 ± 0.46[*†]
Acetyl-CoA carboxylase	ACC	1.27 ± 0.10	0.80 ± 0.05	1.49 ± 0.37[*†]
Sterol regulatory element-binding protein-1	SREBP-1	3.76 ± 0.51[*]	1.93 ± 0.23[‡]	4.69 ± 0.17[*‡†]
Peroxisome proliferator activated receptor γ1	PPARγ1	1.45 ± 0.42	1.58 ± 0.48	1.29 ± 0.26
Peroxisome proliferator activated receptor γ2	PPARγ2	1.88 ± 0.33	12.92 ± 6.04[‡]	50.18 ± 3.61[*‡†]
PPARγ coactivator-1β	PGC-1β	0.81 ± 0.10	0.61 ± 0.15[‡]	0.59 ± 0.12[‡†]
Fatty acid oxidation				
Peroxisome proliferator activated receptor α	PPARα	0.51 ± 0.23	1.25 ± 0.48	1.28 ± 0.41
Carnitine palmitoyl transferase-1	CPT-1	0.63 ± 0.11	1.03 ± 0.34	1.08 ± 0.57
Triglyceride excretion				
Microsomal triglyceride transfer protein	MTP	1.04 ± 0.16	0.92 ± 0.11	0.91 ± 0.11
Apolipoprotein B	ApoB	1.11 ± 0.15	1.20 ± 0.13	1.15 ± 0.09
Cholesterol metabolism				
Sterol regulatory element-binding protein-2	SREBP-2	0.87 ± 0.15	1.66 ± 0.25	1.69 ± 0.34
Hydroxymethylglutaryl-CoA synthase-1	HMGCs1	1.03 ± 0.11	1.60 ± 0.26	4.56 ± 0.73[*‡†]
Hydroxymethylglutaryl-CoA reductase	HMGCr	0.99 ± 0.13	1.22 ± 0.32	2.93 ± 0.44[*‡†]
Apolipoprotein A-1	ApoA1	0.93 ± 0.09	1.26 ± 0.21	0.61 ± 0.11[*‡†]

All results are expressed as the relative fold change compared to the low-fat control diet group ± SD ($n = 6$ per each group).
[*] Significantly different from the corresponding control group with the same dietary composition; $p < 0.05$.
[‡] Significantly different from the low-fat diet with the same dietary lipid as a source; $p < 0.05$.
[†] Significantly different from low-fat control diet group; $p < 0.05$.

Please cite this article in press as: Obara N et al. Possible involvement and the mechanisms of excess *trans*-fatty acid consumption in severe NAFLD in mice. J Hepatol (2010), doi:10.1016/j.jhep.2010.02.029

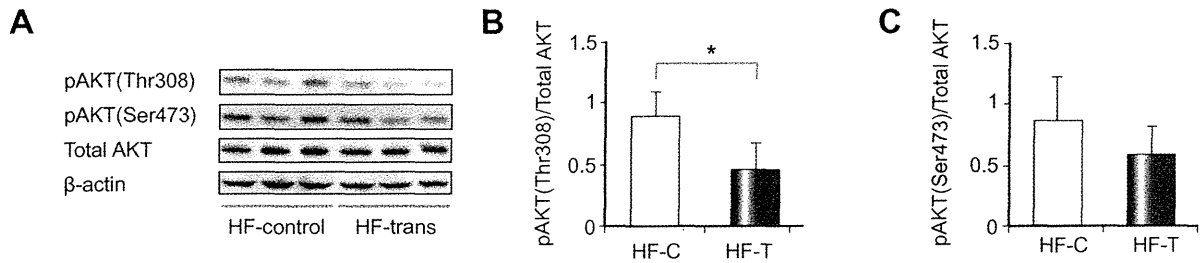

Fig. 3. Effect of excessive TFA consumption of AKT in the high-fat diet-fed mice liver. (A) Representative pictures of phospho-AKT (Thr308 and Ser473), total AKT and β-actin Western blots as well as densitometric analysis of the (B) pAKT(Thr308) or (C) pAKT(Thr473)/total AKT ratio. $^{*}p < 0.05$.

though a few studies have reported that hepatic steatosis [30] and ALT elevation [17] were induced by a TFA-rich diet in mice, the mechanisms remain to be clarified. In agreement with this, the HF-T group showed severe steatosis with a significant transaminase elevation, while HF-C-fed mice only showed moderate steatosis without liver injury, in addition we showed that relatively small amounts of TFA-rich oil intake do not induce severe steatosis and liver injury in the current study. Interestingly, the plasma cholesterol fraction was significantly altered even in the LF-T group in association with the elevation of the total: HDL-cholesterol ratio, a risk factor index of coronary artery disease [22]. The alteration of the plasma cholesterol fraction might be partially explained by changes in the cholesterol metabolism-related gene expressions in the HF-T group, but not in the LF-T group. We could not determine why the cholesterol fraction was altered in the LF-T group, but it might be partially due to the modified membrane fluidity induced by TFA intake [14]. That a relatively small TFA intake could affect the cholesterol fraction but not the liver might be the reason why less attention has been paid to the liver until recently.

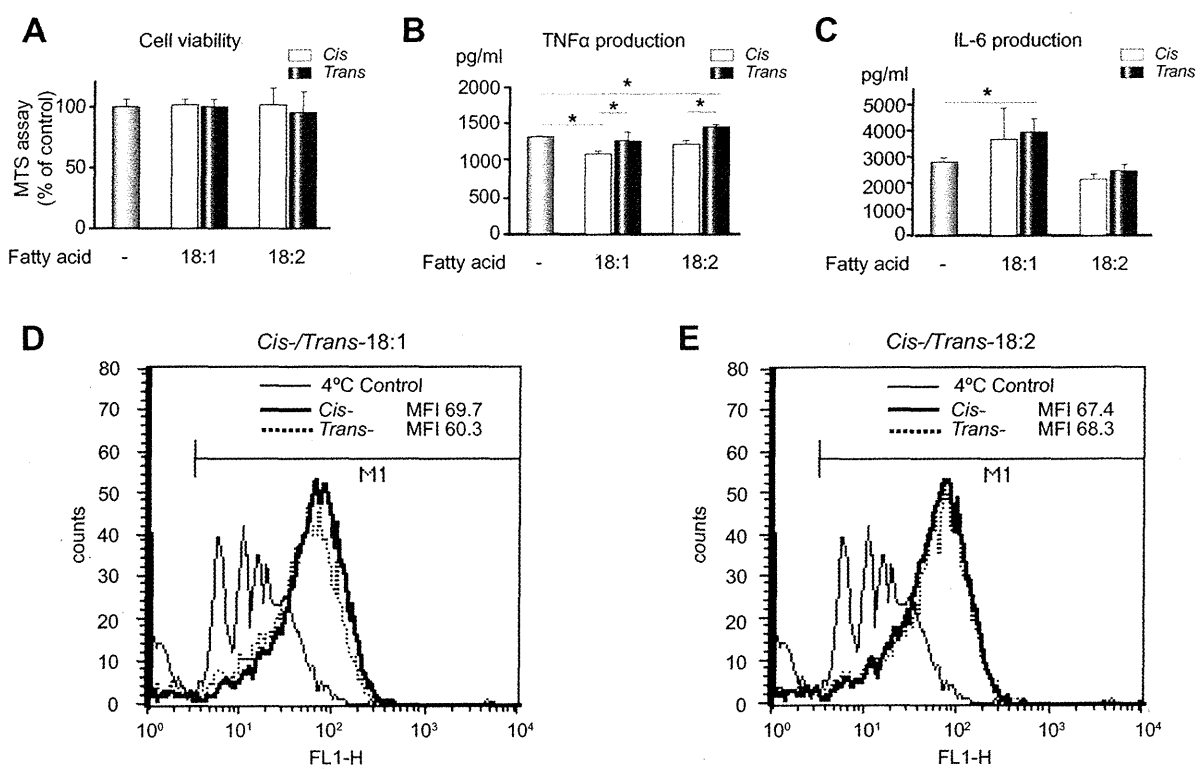

Fig. 4. The impact of *cis*-/*trans*-fatty acid on the cytokine production and phagocytotic ability of KCs. (A) No fatty acids (200 μM) shows cytotoxicity for primary KCs after 24 h incubation, but (B) increases TNFα production in both C18:1 and C18:2-TFA-containing medium compared to its *cis*-structural isomer. (D) IL-6 production increases in C18:1-containing medium and remains unchanged in C18:2-containing medium, whereas the *cis*- or *trans*-structural difference does affect the results. The influence of the C18:1 (D) and C18:2 (E) *cis*-/*trans*-fatty acid on the phagocytotic ability of KCs is measured by flow cytometry analysis. MFI: mean fluorescence intensity ($n = 8$ for each group, A–C). $^{*}p < 0.05$.

Please cite this article in press as: Obara N et al. Possible involvement and the mechanisms of excess *trans*-fatty acid consumption in severe NAFLD in mice. J Hepatol (2010), doi:10.1016/j.jhep.2010.02.029

One of the noted biochemical changes seen in the HF-T group was the elevation of plasma FFA, almost all of which is derived from adipose tissue and accumulates in the liver as TG in a dose-dependent fashion [7]. The increase of plasma FFA might be due to the TFA incorporation in the adipocyte plasma membrane resulting in decreased membrane fluidity, accompanied by increased adipose tissue insulin resistance as evidenced by increased lipolysis, decreased antilipolysis and decreased glucose uptake in rat adipocytes [14]. In addition, in contrast to TG, the circulating FFAs [21] and accumulation of FFAs in liver [32] are known to exert lipotoxicity to hepatocytes, so the significant increase of the plasma FFA in the HF-T group might affect the pathophysiology. On the other hand, hepatic FFA was higher in HF than LF irrespective of the dietary lipid sources, and it was reported that forced high-fat feeding induced NASH in mice, while usual high-fat intake does not [6]. Hepatic FFA accumulation remained unaltered among healthy, NAFLD and NASH subjects liver [24], so it might not be necessary for the progression to NASH but could be a exacerbating factor in the case of excess fat consumption. Therefore, elevated plasma FFA and accumulated hepatic lipid peroxide [23] would contribute synergistically to the liver injury in this model.

A previous study reported that TFA intake decreased the arachidonic acid level and induced insulin resistance in adipose tissue, probably due to the decreased membrane fluidity [14], and the present study also revealed a decrease of the arachidonic acid level in the liver and lower phosphorylation status of AKT which could reflect the hepatic insulin resistant status in the HF-T group. In addition, a human lipidomic analysis of NAFLD/NASH liver described a decrease of arachidonic acid and unaltered levels of precursor linoleic acid, but the study did not address TFA consumption [24]. Although, the mechanisms of the arachidonic acid decrease and involvement in the insulin resistance and progression to NASH remain to be clarified, these common findings might suggest that TFA intake influences both the liver and adipose tissue in a somewhat similar fashion in NASH patients and people who consume excess TFAs.

Typical pathological findings in human NAFLD/NASH patients such as macrovesicular lipid deposit and inflammation are usually identified around zone 3, though the mice liver showed lipid deposits around zone 1 even in the control lipid-fed group. Microvesicular lipid droplets were remarkable in the HF-T group, so it might be difficult to assess the pathological changes using a human scoring system such as NAS. The pathological differences might be due to a specific problem, since the pediatric NAFLD is known to show histological findings around zone 1 [26], which might be related to the dietary habit of consuming excess TFAs from snacks and first food.

Although the expression of proinflammatory cytokines such as TNFα [30] and IL-1β [17] have been shown to be induced in the mice liver by TFA-rich diets, this was not the case in the current study. However, a previous study reported that, among hypercholesterolemic subjects, the production of TNFα by cultured mononuclear cells was increased by a TFA-rich soy bean margarine diet compared with a natural soybean oil diet [12], and we showed KCs increased TNFα production in TFA-containing medium compared to that of *cis*-structural isomer-containing medium. Accordingly, pathophysiological conditions induced by TFA consumption could be partially due to alterations in the monocyte/macrophage ability in proinflammatory cytokine production and phagocytosis, and KCs in particular may play important roles in the local circumstances.

With regard to the adipokines, the adiponectin levels were not changed between the HF-C and HF-T group, but plasma leptin was significantly increased in the HF-T group. Leptin is an appetite-suppressing and body weight-regulating adipokine, and is even related to liver regeneration and fibrosis [13]; hyperleptinemia might be related directly to the elevation of type1 collagen α1 mRNA expression in the liver.

In terms of the severe steatosis of the model, the lipogenetic genes such as FAS, ACC, SREBP-1 and PPARγ2 were coordinately induced, but PGC-1β was not. PGC-1β is known to be induced in the liver by short term high-fat feeding, to coactivate SREBP-1, but to reduce hepatic fat accumulation. However, since it was not investigated in this study, the decrease of PGC-1β gene expression might be due to long term feeding or any other factors, such as the relatively low carbohydrate diet. It was reported that a TFA-rich diet suppressed the PPARγ gene expression in rat adipose tissue [8], and that lipogenic gene expressions in the liver and the adipose tissue are reciprocal modulations [4], which might reflect the core mechanisms of the heterotopic fat accumulation *in vivo*.

In summary, excess TFA consumption induces significant hepatic steatosis accompanied by augmentation of the hepatic lipogenic gene expressions, FFA influx into the liver, and the hepatic accumulation of lipid peroxide. The hepatic accumulation of TFA and the reduction of the arachidonic acid content were the lipidomic properties in this model. Together with their potential induction of local cytokines by KCs, lipid species including TFA may play a pivotal role in the development of non-alcoholic fatty liver diseases.

Acknowledgements

This study was supported in part from Health and Labour Sciences Research Grants for the Research on Measures for Intractable Diseases (from the Ministry of Health, Labour and Welfare of Japan), from Grant-in-Aid for Scientific Research C (20590755 to KF) from Japanese Society of Promotion of Science (JSPS).

Appendix A. Supplementary data

Supplementary data associated with this article can be found, in the online version, at doi:10.1016/j.jhep.2010.02.029.

References

[1] Babior BM. Oxygen-dependent microbial killing by phagocytes (first of two parts). N Engl J Med 1978;298:659–668.
[2] Browning JD, Szczepaniak LS, Dobbins R, Nuremberg P, Horton JD, Cohen JC, et al. Prevalence of hepatic steatosis in an urban population in the United States: impact of ethnicity. Hepatology 2004;40:1387–1395.
[3] Buettner R, Parhofer KG, Woenckhaus M, Wrede CE, Kunz-Schughart LA, Scholmerich J, et al. Defining high-fat-diet rat models: metabolic and molecular effects of different fat types. J Mol Endocrinol 2006;36:485–501.
[4] Cao H, Gerhold K, Mayers JR, Wiest MM, Watkins SM, Hotamisligil GS. Identification of a lipokine, a lipid hormone linking adipose tissue to systemic metabolism. Cell 2008;134:933–944.
[5] Day CP, James OF. Steatohepatitis: a tale of two "hits"? Gastroenterology 1998;114:842–845.

Please cite this article in press as: Obara N et al. Possible involvement and the mechanisms of excess *trans*-fatty acid consumption in severe NAFLD in mice. J Hepatol (2010), doi:10.1016/j.jhep.2010.02.029

[6] Deng QG, She H, Cheng JH, French SW, Koop DR, Xiong S, et al. Steatohepatitis induced by intragastric overfeeding in mice. Hepatology 2005;42:905–914.
[7] Donnelly KL, Smith CI, Schwarzenberg SJ, Jessurun J, Boldt MD, Parks EJ. Sources of fatty acids stored in liver and secreted via lipoproteins in patients with nonalcoholic fatty liver disease. J Clin Invest 2005;115:1343–1351.
[8] Duque-Guimaraes DE, de Castro J, Martinez-Botas J, Sardinha FL, Ramos MP, Herrera E, et al. Early and prolonged intake of partially hydrogenated fat alters the expression of genes in rat adipose tissue. Nutrition 2009;25: 782–789.
[9] Farrell GC, Larter CZ. Nonalcoholic fatty liver disease: from steatosis to cirrhosis. Hepatology 2006;43:S99–S112.
[10] Folch J, Lees M, Sloane Stanley GH. A simple method for the isolation and purification of total lipides from animal tissues. J Biol Chem 1957;226: 497–509.
[11] Gonzalez-Periz A, Horrillo R, Ferre N, Gronert K, Dong B, Moran-Salvador E, et al. Obesity-induced insulin resistance and hepatic steatosis are alleviated by omega-3 fatty acids: a role for resolvins and protectins. FASEB J 2009;23:1946–1957.
[12] Han SN, Leka LS, Lichtenstein AH, Ausman LM, Schaefer EJ, Meydani SN. Effect of hydrogenated and saturated, relative to polyunsaturated, fat on immune and inflammatory responses of adults with moderate hypercholesterolemia. J Lipid Res 2002;43:445–452.
[13] Honda H, Ikejima K, Hirose M, Yoshikawa M, Lang T, Enomoto N, et al. Leptin is required for fibrogenic responses induced by thioacetamide in the murine liver. Hepatology 2002;36:12–21.
[14] Ibrahim A, Natrajan S, Ghafoorunissa R. Dietary trans-fatty acids alter adipocyte plasma membrane fatty acid composition and insulin sensitivity in rats. Metabolism 2005;54:240–246.
[15] Kechagias S, Ernersson A, Dahlqvist O, Lundberg P, Lindstrom T, Nystrom FH. Fast-food-based hyper-alimentation can induce rapid and profound elevation of serum alanine aminotransferase in healthy subjects. Gut 2008;57:649–654.
[16] Kleiner DE, Brunt EM, Van Natta M, Behling C, Contos MJ, Cummings OW, et al. Design and validation of a histological scoring system for nonalcoholic fatty liver disease. Hepatology 2005;41:1313–1321.
[17] Koppe SW, Elias M, Moseley RH, Green RM. Trans fat feeding results in higher serum alanine aminotransferase and increased insulin resistance compared with a standard murine high-fat diet. Am J Physiol Gastrointest Liver Physiol 2009;297:G378–G384.
[18] Larter CZ, Yeh MM, Haigh WG, Williams J, Brown S, Bell-Anderson KS, et al. Hepatic free fatty acids accumulate in experimental steatohepatitis: role of adaptive pathways. J Hepatol 2008;48:638–647.
[19] Lin J, Yang R, Tarr PT, Wu PH, Handschin C, Li S, et al. Hyperlipidemic effects of dietary saturated fats mediated through PGC-1beta coactivation of SREBP. Cell 2005;120:261–273.
[20] Lopez-Garcia E, Schulze MB, Meigs JB, Manson JE, Rifai N, Stampfer MJ, et al. Consumption of trans fatty acids is related to plasma biomarkers of inflammation and endothelial dysfunction. J Nutr 2005;135:562–566.
[21] Malhi H, Gores GJ. Molecular mechanisms of lipotoxicity in nonalcoholic fatty liver disease. Semin Liver Dis 2008;28:360–369.
[22] Mensink RP, Zock PL, Kester AD, Katan MB. Effects of dietary fatty acids and carbohydrates on the ratio of serum total to HDL cholesterol and on serum lipids and apolipoproteins: a meta-analysis of 60 controlled trials. Am J Clin Nutr 2003;77:1146–1155.
[23] Milagro FI, Campion J, Martinez JA. Weight gain induced by high-fat feeding involves increased liver oxidative stress. Obesity (Silver Spring) 2006;14: 1118–1123.
[24] Puri P, Baillie RA, Wiest MM, Mirshahi F, Choudhury J, Cheung O, et al. A lipidomic analysis of nonalcoholic fatty liver disease. Hepatology 2007;46:1081–1090.
[25] Reid AE. Nonalcoholic steatohepatitis. Gastroenterology 2001;121:710–723.
[26] Schwimmer JB, Behling C, Newbury R, Deutsch R, Nievergelt C, Schork NJ, et al. Histopathology of pediatric nonalcoholic fatty liver disease. Hepatology 2005;42:641–649.
[27] Shimano H, Horton JD, Hammer RE, Shimomura I, Brown MS, Goldstein JL. Overproduction of cholesterol and fatty acids causes massive liver enlargement in transgenic mice expressing truncated SREBP-1a. J Clin Invest 1996;98:1575–1584.
[28] Su GL, Klein RD, Aminlari A, Zhang HY, Steinstraesser L, Alarcon WH, et al. Kupffer cell activation by lipopolysaccharide in rats: role for lipopolysaccharide binding protein and toll-like receptor 4. Hepatology 2000;31: 932–936.
[29] Sun Q, Ma J, Campos H, Hankinson SE, Manson JE, Stampfer MJ, et al. A prospective study of trans fatty acids in erythrocytes and risk of coronary heart disease. Circulation 2007;115:1858–1865.
[30] Tetri LH, Basaranoglu M, Brunt EM, Yerian LM, Neuschwander-Tetri BA. Severe NAFLD with hepatic necroinflammatory changes in mice fed trans fats and a high-fructose corn syrup equivalent. Am J Physiol Gastrointest Liver Physiol 2008;295:G987–G995.
[31] Tsuzuki T, Tokuyama Y, Igarashi M, Nakagawa K, Ohsaki Y, Komai M, et al. Alpha-eleostearic acid (9Z11E13E-18:3) is quickly converted to conjugated linoleic acid (9Z11E-18:2) in rats. J Nutr 2004;134:2634–2639.
[32] Yamaguchi K, Yang L, McCall S, Huang J, Yu XX, Pandey SK, et al. Inhibiting triglyceride synthesis improves hepatic steatosis but exacerbates liver damage and fibrosis in obese mice with nonalcoholic steatohepatitis. Hepatology 2007;45:1366–1374.
[33] Zhang YL, Hernandez-Ono A, Siri P, Weisberg S, Conlon D, Graham MJ, et al. Aberrant hepatic expression of PPARgamma2 stimulates hepatic lipogenesis in a mouse model of obesity, insulin resistance, dyslipidemia, and hepatic steatosis. J Biol Chem 2006;281:37603–37615.

Please cite this article in press as: Obara N et al. Possible involvement and the mechanisms of excess *trans*-fatty acid consumption in severe NAFLD in mice. J Hepatol (2010), doi:10.1016/j.jhep.2010.02.029

Biochemical and Biophysical Research Communications xxx (2011) xxx–xxx

Contents lists available at ScienceDirect

Biochemical and Biophysical Research Communications

journal homepage: www.elsevier.com/locate/ybbrc

AMSH is required to degrade ubiquitinated proteins in the central nervous system

Shunya Suzuki [a], Keiichi Tamai [a,d,*], Masahiko Watanabe [e], Masanao Kyuuma [a], Masao Ono [c], Kazuo Sugamura [a,d], Nobuyuki Tanaka [b,d]

[a] Department of Microbiology and Immunology, Tohoku University Graduate School of Medicine, Sendai 980-8575, Japan
[b] Department of Cancer Science, Tohoku University Graduate School of Medicine, Sendai 980-8575, Japan
[c] Department of Pathology, Tohoku University Graduate School of Medicine, Sendai 980-8575, Japan
[d] Division of Immunology, Miyagi Cancer Center Research Institute, Natori 981-1293, Japan
[e] Department of Anatomy, Hokkaido University School of Medicine, Sapporo 060-8638, Japan

ARTICLE INFO

Article history:
Received 14 April 2011
Available online xxxx

Keywords:
AMSH
Neurodegeneration
Ubiquitin
Hippocampus

ABSTRACT

Deubiquitination is a biochemical process that mediates the removal of ubiquitin moieties from ubiquitin-conjugated substrates. AMSH (associated molecule with the SH3 domain of STAM) is a deubiquitination enzyme that participates in the endosomal sorting of several cell-surface molecules. AMSH impairment results in missorted ubiquitinated cargoes *in vitro* and severe neurodegeneration *in vivo*, but it is not known how AMSH deficiency causes neuronal damage in the brain. Here, we demonstrate that AMSH$^{-/-}$ mice developed ubiquitinated protein accumulations as early as embryonic day 10 (E10), and that severe deposits were present in the brain at postnatal day 8 (P8) and P18. Interestingly, TDP-43 was found to accumulate and colocalize with glial marker-positive cells in the brain. Glutamate receptor and p62 accumulations were also found; these molecules colocalized with ubiquitinated aggregates in the brain. These data suggest that AMSH plays an important role in degrading ubiquitinated proteins and glutamate receptors *in vivo*. AMSH$^{-/-}$ mice provide an animal model for neurodegenerative diseases, which are commonly characterized by the generation of proteinaceous aggregates.

1. Introduction

The highly dynamic endosomal sorting process determines a membrane-bound protein's fate by either recycling it back to the cell surface or delivering it into endosomal network pathways. Membrane proteins destined for lysosomes are tagged with ubiquitin. Endosomal sorting complexes required for transport (ESCRT) recognizes and dictates cargo selection. ESCRT produces intraluminal vesicles (ILVs) that originate by inward budding from the limiting membrane of the sorting endosome [1]. This process creates a multivesicular body (MVB), which leads to lysosome-dependent cargo degradation through the subsequent MVB-lysosome fusion event.

Balanced ubiquitination and deubiquitination of cargos is a prerequisite for protein homeostasis. Ubiquitin modifications are reversed through the isopeptidase activities of deubiquitinating enzymes (DUBs), with most of the DUBs studied deconjugating only a small number of targets [2]. In fact, deubiquitination, a term used here to refer to both ubiquitin and ubiquitin-like deconjugation, is emerging as a regulatory process in signaling pathways, chromatin structure, endocytosis, and apoptosis [2], and is important for physiological activities such as development, immunity, and neuronal function [3].

We identified AMSH (associated molecule with the SH3 domain of STAM) [4] while screening for an ESCRT-bound molecule. AMSH is an endosomal DUB in the JAMM metalloprotease family, and plays a role in MVB/late endosomes. Recombinant AMSH has been shown to deubiquitinate epidermal growth factor receptor (EGFR) and to cleave lysine 63 (K63)-linked, but not lysine 48 (K48)-linked, polyubiquitin chains into ubiquitin monomers [5]. In a previous study, we found that AMSH binds the ESCRT-III subunit CHMP3 and plays a role in MVB/late endosomes [6]. AMSH also binds the ESCRT-III subunits CHMP1A, CHMP1B, and CHMP2A [7]. This intimate relationship between AMSH and ESCRT prompted us to investigate AMSH's *in vivo* roles. We have reported that AMSH knockout mice (AMSH$^{-/-}$) exhibit postnatal growth retardation and die between postnatal day 19 (P19) and P23. AMSH$^{-/-}$ mice exhibit severe neuronal damage, specifically neuron loss and increasing numbers of apoptotic cells, that is almost en-

Abbreviations: AD, Alzheimer's disease; ALS, amyotrophic lateral sclerosis; AMSH, associated molecule with the SH3 domain of STAM; AMPAR, α-amino-3-hydroxy-5-methyl-isoxazolepropionic acid receptor; CHMP, chromatin modifying protein; ESCRT, endosomal sorting complexes required for transport; FTD, frontotemporal dementia; MVB, multivesicular body; NMDAR, *N*-methyl-D-aspartate receptor; PD, Parkinson's disease; DUB, deubiquitinating enzyme.

* Corresponding author at: Division of Immunology, Miyagi Cancer Center Research Institute, 47-1 Nodayama, Medeshima-Shiode, Natori, Miyagi 981-1293, Japan. Fax: +81 22 381 1168.
E-mail address: tamaikeiichi@mac.com (K. Tamai).

0006-291X/$ - see front matter © 2011 Elsevier Inc. All rights reserved.
doi:10.1016/j.bbrc.2011.04.065

tirely confined to the CA1 subfield of the hippocampus [8]. Despite the severity of these AMSH-deficient neuronal phenotypes, the pathophysiology is not fully understood.

Most age-related neurodegenerative diseases are characterized by accumulations of aberrant protein aggregates in affected regions of the brain. In particular, ubiquitin-positive proteinaceous deposits are a hallmark of neurodegeneration; such deposits include Lewy bodies in Parkinson's disease (PD), neurofibrillary tangles in Alzheimer disease (AD), Bunina bodies in amyotrophic lateral sclerosis (ALS), and Pick bodies in frontotemporal dementia (FTD) with parkinsonism [9]. Since principal function of ubiquitination is to maintain protein homeostasis inside a cell, these neuronal pathologies may indicate a failure to clear unwanted proteins [9]. A recent report suggests that ESCRT-III dysfunction is associated with neurodegeneration resembling age-dependent neurodegenerative diseases such as FTD [10]. A certain percentage of FTD is known as chromosome 3-linked FTD (FTD3), which is attributed to a genetic disorder or mutation of the ESCRT-III molecule CHMP2B [11]. In a previous study using neuron-specific knockout mice, we found that the ESCRT-0 protein Hrs plays a pivotal role in neural cell survival by clearing ubiquitinated proteins in neurons [12]. A growing body of evidence suggests that insufficient ESCRT function leads to the accumulation of ubiquitinated proteins and to human neurodegenerative disease [13]. Nevertheless, little is known about how an ESCRT-associating DUB is involved in ubiquitinated protein degradation in the central nervous system. Here, we demonstrate that ubiquitinated protein accumulations are present in brain lesions found in AMSH$^{-/-}$ mice, and that AMSH is crucial for the proper degradation of both ubiquitinated proteins and glutamate receptors in the central nervous system.

2. Materials and methods

2.1. Cell fractionation

Cerebral tissues were washed with phosphate-buffered saline (PBS), suspended with homogenization buffer (10 mM HEPES, 3 mM imidazole, and 250 mM sucrose), and dissociated by passage through a 22-G needle. The cells were centrifuged at 3000*g* for 10 min at 4 °C, and the supernatants were ultracentrifuged at 100,000*g* for 30 min at 4 °C. The supernatants were regarded as the cytoplasmic fraction, and the pellets as the membrane fraction. The pellets were resuspended with IP buffer (10 mM Hepes, pH 7.2, 0.5% Triton-X, 150 mM NaCl) and centrifuged at 10,000*g* for 30 min at 4 °C. The supernatants were filtered through a polyvinylidene difluoride (PVDF) membrane (0.45 μm, PALL Life Sciences, NY) and regarded as a membrane fraction. These fractions were quantified using the Bio-Rad Protein assay (Bio-Rad, CA) according to the manufacturer's protocol.

2.2. Western blotting

Immunoblotting was conducted as previously described [4]. In brief, mouse brain lysates were fractionated as described above, then separated by sodium dodecyl sulfate–polyacrylamide gel electrophoresis (SDS–PAGE) and transferred onto PVDF membranes (Millipore, MA). After being blocked with 5% nonfat milk in Tris-buffered saline (TBS) containing 0.1% Tween 20, the membranes were probed with the primary antibodies indicated below, washed again, and probed with horseradish peroxidase (HRP)-conjugated secondary antibodies (Cell Signaling, MA).

2.3. Immunofluorescence reactions and immunohistochemistry

For immunofluorescence studies, mice were perfused with 4% paraformaldehyde, and 50-μm sections were prepared using a microslicer (VT1000S, Leica, Nussloch, Germany). The antibodies and dilutions used were as follows: Anti-ubiquitin mouse monoclonal Ab (mAb) 1B3 (MBL, Nagoya, Japan), 1:100; anti-ubiquitin mouse mAb FK2 (BIOMOL, NY), 1:100; anti-TDP-43 mouse mAb (TARDBP) (Proteintech Group, IL), 1:100; anti-p62 (C-terminal specific) guinea pig polyclonal antibody (pAb) (American Research Products, MA), 1:100; anti-GFAP mouse mAb (Chemicon, CA), 1:200; anti-tyrosine hydroxylase rabbit pAb (AB152, Chemicon), 1:1000; anti-microtubule-associated protein 2 goat pAb (MAP2, [14]), 1 μg/mL; anti-calbindin rabbit pAb [15], 1 μg/mL. Appropriately, coupled secondary antibodies (Alexa Fluor, Molecular Probes, CA) were used for double-labeling. For immunohistochemistry, we used the Histofine mouse stain kit or Histofine simple stain mouse MAX-PO(R) (Nichirei, Japan), according to the manufacturer's protocols.

3. Results

Because AMSH is a deubiquitinating enzyme with endosome functions, we analyzed ubiquitinated protein accumulation in the soluble (cytoplasmic) and insoluble (membrane) fractions of the AMSH$^{-/-}$ brain. Western blot analysis using the anti-ubiquitin antibody P4D1 revealed no difference in ubiquitinated protein levels in the soluble fractions from control or AMSH$^{-/-}$ brains (Fig. 1, left panels). In the insoluble fraction, however, the ubiquitinated protein levels were higher in the AMSH$^{-/-}$ brain than in the control (Fig. 1, right panels). The ubiquitinated protein levels in the insoluble fraction increased slightly from embryonic day 10 (E10) to postnatal day 8 (P8) in the control brain, and the levels were higher in the AMSH$^{-/-}$ than the control brain during E10 to P18, near the end of the AMSH$^{-/-}$ mouse lifespan. By P8 the ubiquitinated protein levels in the AMSH$^{-/-}$ brain had increased markedly. These data suggest that AMSH deficiency leads to the progressive accumulation of ubiquitinated proteins in the membrane fraction of the brain.

Histopathological examination of the hippocampus, the brain region most affected in AMSH$^{-/-}$ mice, showed evident neurodegeneration in the CA1 subfield in P6 mice [8]. Confirming the pres-

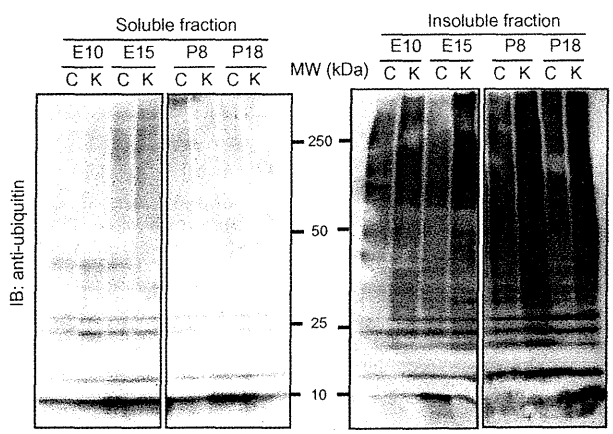

Fig. 1. Ubiquitinated proteins increase with aging in the AMSH knockout mouse brain. Western blots were performed on soluble and insoluble brain fractions of control (C) and AMSH knockout (K) mice at the ages indicated (see Section 2) using the anti-ubiquitin antibody P4D1. Gels were loaded with equal amounts of protein. IB, immunoblotting.

Please cite this article in press as: S. Suzuki et al., AMSH is required to degrade ubiquitinated proteins in the central nervous system, Biochem. Biophys. Res. Commun. (2011), doi:10.1016/j.bbrc.2011.04.065

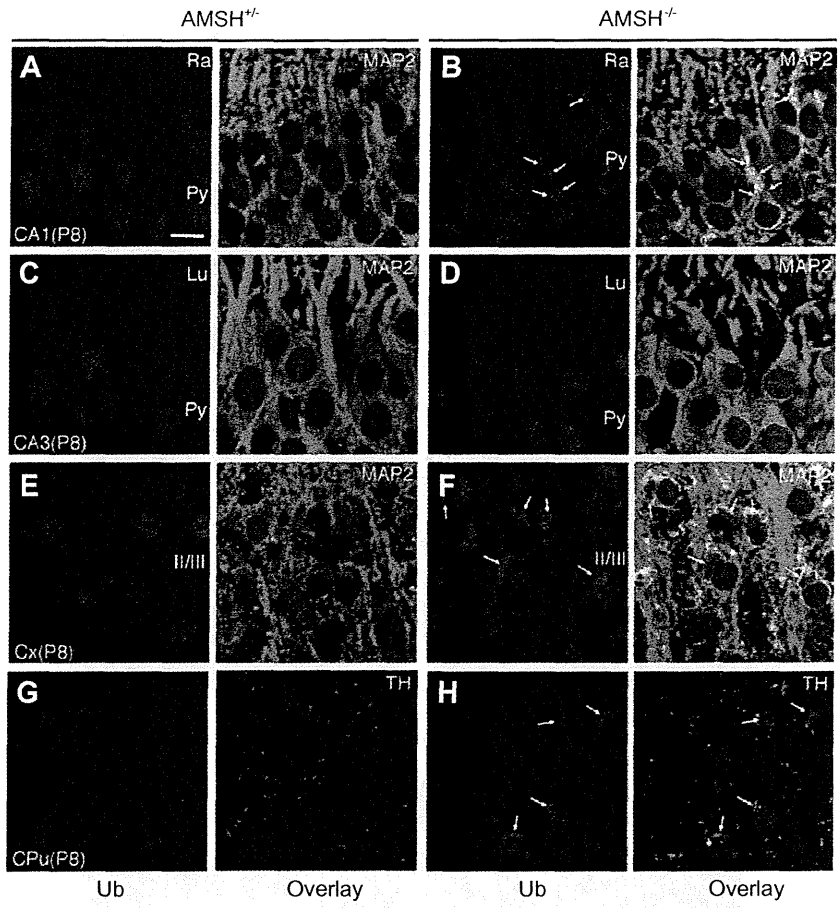

Fig. 2. Ubiquitinated proteins accumulate in the AMSH$^{-/-}$ mouse neurons. Immunofluorescence in postnatal day 8 (P8) AMSH$^{+/-}$ and AMSH$^{-/-}$ tissues stained with antibodies against ubiquitinated proteins in red (clone FK2) is shown in the hippocampal CA1 (A and B), CA3 (C and D), cerebral cortex (E and F), and caudate putamen (G and H). Arrows indicate ubiquitin-positive aggregates. Bar, 10 μm. Lu, stratum lucidum; Py, pyramidal cell layer; Ra, stratum radiatum; II/III, laminae II/III.

ence of neural damage, staining with the glial marker GFAP (glial fibrillary acidic protein) was greater in the hippocampal CA1 subfield of the AMSH$^{-/-}$ P1 brain than in the control, and was profoundly increased in P8 mice (data not shown). To determine whether ubiquitin is involved in the neuronal degeneration observed in AMSH$^{-/-}$ mice, we immunostained brain tissues with FK2, an antibody against ubiquitinated protein. In P8 AMSH$^{-/-}$ brains, FK2-stained granules were clearly apparent in the CA1 subfield, frontal cortex (Cx), and caudate putamen (CPu), but not in the CA3 subfield (Fig. 2A to H in red). The immunostainings of microtubule-associated protein 2 and ubiquitined aggregate were colocalized in CA1 and Cx (Fig. 2A–F). The staining patterns both dopaminergic (tyrosine hydroxylase-positive) fibers in CPu were similar between control and AMSH$^{-/-}$ mice (Fig. 2G and H). The ubiquitinated aggregates in CPu were partially colocalized with dopaminergic fibers, which suggested that ubiquitinated proteins did not accumulated in dopaminergic neurons but in the striatal neurons receiving dopaminergic input. These results suggested that both the ubiquitinated protein accumulation and neuron loss specifically occurred in the AMSH$^{-/-}$ CA1 subfield.

We next examined whether the AMSH deficiency impacts autophagy. Because AMSH is generally known to interact with ESCRT protein components [16], and ESCRT is closely involved with the autophagic pathway [12,17], insufficient autophagy and autophagic protein clearance might account for the aggregation of ubiquitinated proteins in the AMSH$^{-/-}$ mouse brain. We therefore looked at two marker proteins for autophagy: LC3, a specific autophagosome marker, and p62, a ubiquitin-binding protein that is implicated in autophagic protein degradation and that accumulates intracellularly with insufficient autophagy [18]. Although LC3-positive vesicles could not be detected at P20 in either the control or AMSH$^{-/-}$ brain (data not shown), p62 aggregations were clearly observed in pyramidal cell perikarya in the CA1 subfield, Cx, and CPu in the AMSH$^{-/-}$ brain (Fig. 3A and B in red[1] and data not shown). Notably, p62 and ubiquitinated proteins colocalized strongly.

We next examined the expression of the transactivation response element (TAR)-DNA-binding protein 43 (TDP-43), since a previous report suggested that defective ESCRT function leads to aggregations of cytoplasmic proteins, including TDP-43 [19]. Interestingly, TDP-43 was found in several regions of the AMSH$^{-/-}$ P8 brain, including the CA1 subfield, Cx, and CPu (Fig. 3E and F in green and data not shown), and its levels increased markedly from P8 to P20 (Fig. 3G and H). TDP-43 accumulations did not colocalize with ubiquitinated proteins (Fig. 3F), but rather with GFAP (Fig. 3D). These data indicate that TDP-43 accumulates in astrocytes but not neural cells in AMSH$^{-/-}$ mice.

AMSH is known to deubiquitinate receptors, such as the EGF receptor [5] and protease-activated receptor 2 [20], but how AMSH contributes to receptor deubiquitination *in vivo* is unknown. We

[1] For interpretation of color in Figs. 2 and 3, the reader is referred to the web version of this article.

Please cite this article in press as: S. Suzuki et al., AMSH is required to degrade ubiquitinated proteins in the central nervous system, Biochem. Biophys. Res. Commun. (2011), doi:10.1016/j.bbrc.2011.04.065

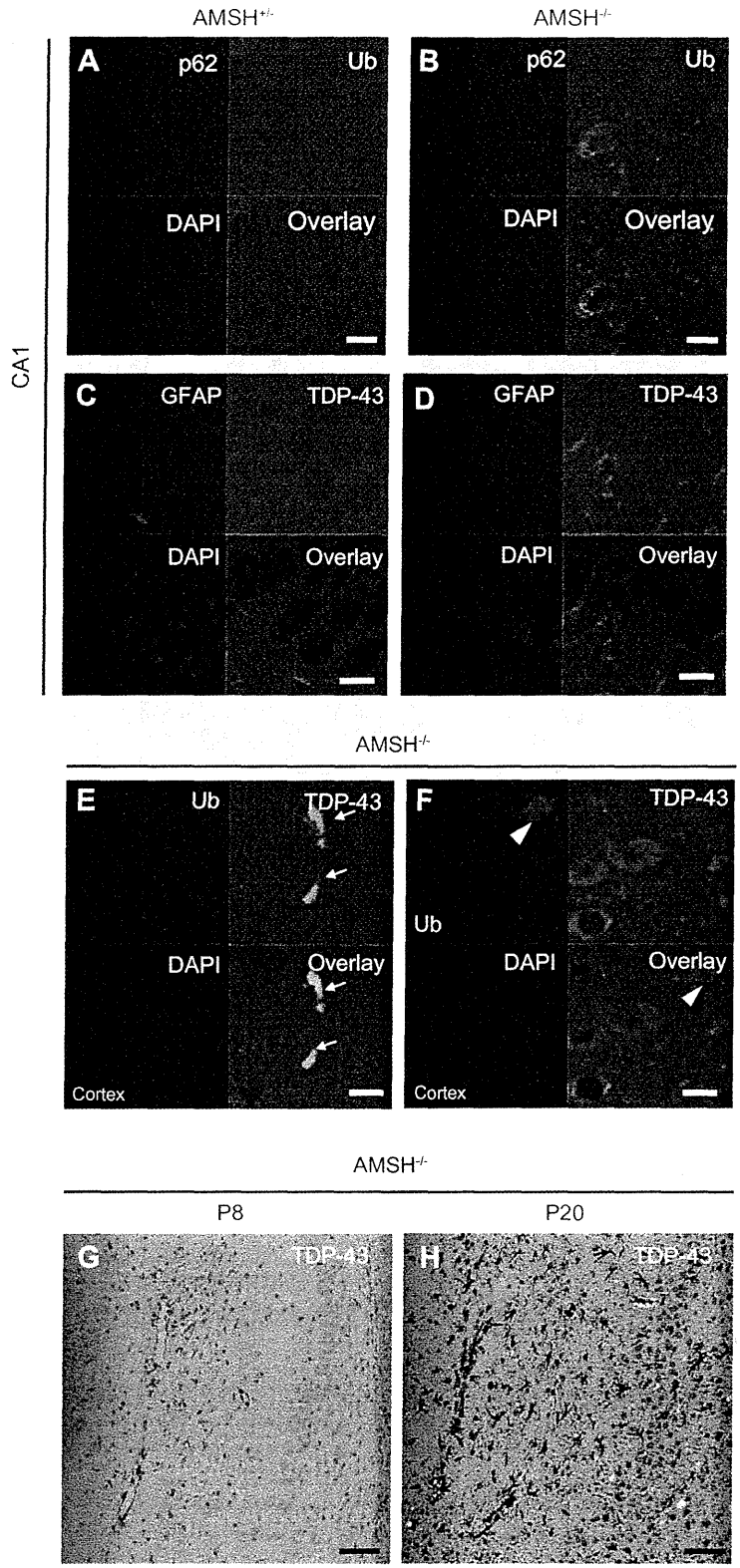

Fig. 3. Ubiquitinated proteins, p62, and TDP-43 accumulate in the AMSH $^{-/-}$ mouse brain. (A and B) Immunofluorescence in P20 AMSH$^{+/-}$ and AMSH$^{-/-}$ tissues stained with antibodies against ubiquitinated proteins (1B3) and p62 is shown in the hippocampal CA1. (C and D) TDP-43 and GFAP colocalize in the AMSH$^{-/-}$ mouse brain. Immunofluorescence staining with antibodies against GFAP and TDP-43 in AMSH$^{+/-}$ and AMSH $^{-/-}$ mice at P20 in the hippocampal CA1 subfield. Bar, 10 μm. (E and F) Immunofluorescence staining in the cerebral cortex of P20 AMSH$^{+/-}$ and AMSH $^{-/-}$ mice, using antibodies against ubiquitinated proteins (1B3) and TDP-43. Arrows indicate TDP-43-positive cells. Arrowheads indicate ubiquitin-positive cells. Bar, 10 μm. (G and H) Immunohistochemistry of hippocampal CA1 subfields from AMSH$^{-/-}$ mice at P8 (E) and P20 (F), stained with an anti-TDP-43 antibody. Bar, 50 μm.

Please cite this article in press as: S. Suzuki et al., AMSH is required to degrade ubiquitinated proteins in the central nervous system, Biochem. Biophys. Res. Commun. (2011), doi:10.1016/j.bbrc.2011.04.065

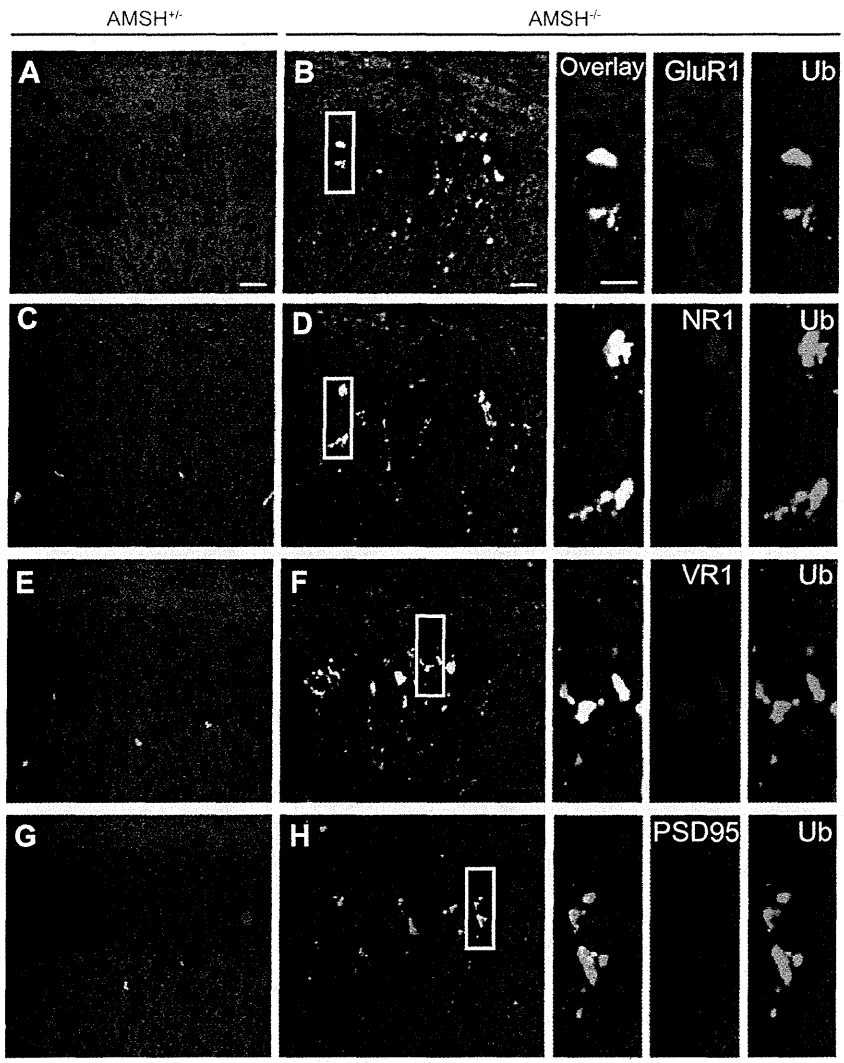

Fig. 4. Patterns of glutamate receptor subunits and ubiquitinated proteins. Immunofluorescence reactions in P8 AMSH$^{+/-}$ (A, C, E, G) and AMSH$^{-/-}$ (B, D, F, H) mice are shown. CA1 subfields were counterstained with DAPI (blue) and stained with antibodies (red) against GluR1 (A and B), NR1 (C and D), VR1 (E and F), and PSD95 (G and H). Ubiquitinated proteins were also stained in green.

suspected that glutamate receptors, which play prominent roles in several neurodegenerative diseases [21], might be regulated by AMSH. We used immunohistochemistry to examine the expression and localization of GluR1, which is a subunit of the α-amino-3-hydroxy-5-methyl-isoxazolepropionic acid receptor (AMPAR), as well as NR1 and VR1, which are subunits of the *N*-methyl-D-aspartate receptor (NMDAR), in the CA1 subfield. Aggregates in the AMSH$^{+/-}$ brain were not stained by antibodies against GluR1, NR1, or VR1 (Fig. 4A, C, E, and G); however, glutamate receptor-positive aggregates were clearly visible (Fig. 4B, D, F, and H). PSD95, which is known to bind Hrs and control glutaminergic synapse function, was weakly detected and was found colocalized with ubiquitinated proteins. Interestingly, we found the colocalization of glutamate receptor- and ubiquitin-positive aggregates (Fig. 4B, D, F, and H, insets). These results indicate that AMSH is critical for glutamate receptor regulation.

4. Discussion

The present study demonstrated that ubiquitinated proteins were accumulated in the membranous fractions of the AMSH-deficient mouse brain, indicating that membrane traffic is altered. These accumulations were found as early as E10. In a previous study, we found neuron loss in the AMSH-deficient CA1 subfield on and after P8, but not at E19 or P1 [8]. Ubiquitinated protein aggregates in neurons are known to induce neurodegeneration in conditions such as AD, FTD, and ALS [9]. Therefore, it is reasonable that we detected aggregates of ubiquitinated proteins prior to neurodegeneration in the AMSH-deficient brain. Ubiquitinated proteinaceous aggregates in the brains of AMSH-knockout mice colocalized with p62, which also accumulates in the affected neurons. The protein p62 binds ubiquitin and the autophagosome marker protein LC3, and regulates aggregate formation [22]. In addition, p62 is a selective target of autophagy, and is eventually degraded in lysosomes as a result of the autophagosome-lysosome fusion event [22]. Based on these findings, it is possible that AMSH is required for the basal or naturally occurring autophagic clearance of aggregate-prone proteins by facilitating the autophagosome-lysosome fusion.

We also observed TDP-43 aggregates in GFAP-positive glial cells in the AMSH-deficient brain, and these aggregates were not stained by anti-ubiquitin antibodies. In contrast, TDP-43 has been

Please cite this article in press as: S. Suzuki et al., AMSH is required to degrade ubiquitinated proteins in the central nervous system, Biochem. Biophys. Res. Commun. (2011), doi:10.1016/j.bbrc.2011.04.065

reported to accumulate in cytoplasmic lesions in neural cells and to colocalize with ubiquitin-positive cellular inclusions in human neurodegenerative diseases such as ALS and FTD [23]. However, a recent study showed that neuronal and glial inclusions were positively stained with ubiquitin and TDP-43 antibodies in some FTD brain specimens [24]. As TDP-43 is known to be polyubiquitinated in the presence of proteasome inhibitors [25], we expected AMSH to be critical for degrading TDP-43 in glial cells. However, we failed to detect TDP-43 ubiquitination in glial cells. Furthermore, we also examined alpha-synuclein, one of the proteins affected in PD, and phosphorylated Tau, which accumulates in AD, and found no differences between the AMSH$^{+/-}$ and AMSH$^{-/-}$ brains (data not shown). These results suggest that there may be an unknown substrate that needs to be cleared by AMSH-dependent deubiquitination and sorting, or that AMSH may be required for non-specific clearance of unwanted proteins. Further study is required to find AMSH substrates related to neurodegenerative disease.

In contrast to our present findings of neurodegeneration in the CA1 subfield in AMSH knockout mice, we previously reported finding CA3 sector neurodegeneration in STAM1-knockout as well as neuron-specific Hrs-knockout mice [12,26]. STAM1 and Hrs form an ESCRT-0 complex, which sorts ubiquitinated proteins upstream of ESCRT-III [27]. The mechanism determining the specificity of neurodegeneration in CA1 versus CA3 is an intriguing issue. Since AMSH and Hrs are distributed ubiquitously in the hippocampus, including the CA1 and CA3 subfields [8,12], their expression patterns do not account for the difference. The glutamate receptor subunit aggregates that we found in the CA1 subfield of the AMSH$^{-/-}$ brain in this study have also been found in the CA3 subfield in the Hrs-knockout brain. While we cannot completely exclude the possibility that neurodegeneration itself causes the accumulations of ubiquitinated aggregates, we suspect that instead, neurodegeneration is a result of impaired glutamate receptor regulation; we found that ubiquitinated protein accumulations were already present at E10 and E15 in the AMSH$^{-/-}$ brain, before CA1 pyramidal neuron loss occurs [8]. We also suspect that the survival of hippocampal neurons in the CA1 and CA3 subfields requires novel, distinct proteins that are subject to ubiquitination. Further study is required to determine how endosomal trafficking is regulated in the different subfields in the hippocampus.

Among the ESCRT molecules, CHMP2B mutations cause chromosome 3-linked, familial FTD (FTD-3) in humans. CHMP2B is a component of ESCRT-III, and like AMSH, is recruited to the endosomes and MVB for cargo sorting. Because AMSH binds indirectly with CHMP2B via another ESCRT-III molecule, CHMP3 [28], AMSH depletion and CHMP2B mutations seem to share similar pathological features. Indeed, neurodegeneration in FTD-3 patients is distributed not only in the frontal, parietal and temporal cortex, but also in the hippocampus. Histopathological changes found in patients with late stages of ubiquitin-positive FTD include changes in the CA1 sector of the hippocampus [29]. In addition, p62 and ubiquitinated protein accumulations are related to human neurodegenerative diseases [18]. It is not known whether AMSH selectively recognizes harmful gene products associated with neurodegenerative disorders. However, AMSH mutant mice provide an excellent animal model system for studying the molecular mechanisms of neurodegenerative diseases.

Acknowledgments

This work was supported by JSPS and MEXT KAKENHI (21590517, 19059001, and 22790630), by a Grant-in-Aid from the Ministry of Health, Labor and Welfare, by Takeda Medical Research Foundation, and by Intelligent Cosmos Research Institute.

References

[1] J.H. Hurley, S.D. Emr, The ESCRT complexes: structure and mechanism of a membrane-trafficking network, Annu. Rev. Biophys. Biomol. Struct. 35 (2006) 277–298.
[2] S.M. Nijman, M.P. Luna-Vargas, A. Velds, T.R. Brummelkamp, A.M. Dirac, T.K. Sixma, R. Bernards, A genomic and functional inventory of deubiquitinating enzymes, Cell 123 (2005) 773–786.
[3] P.C. Evans, Regulation of pro-inflammatory signalling networks by ubiquitin: identification of novel targets for anti-inflammatory drugs, Expert Rev. Mol. Med. 7 (2005) 1–19.
[4] N. Tanaka, K. Kaneko, H. Asao, H. Kasai, Y. Endo, T. Fujita, T. Takeshita, K. Sugamura, Possible involvement of a novel STAM-associated molecule "AMSH" in intracellular signal transduction mediated by cytokines, J. Biol. Chem. 274 (1999) 19129–19135.
[5] J. McCullough, M.J. Clague, S. Urbe, AMSH is an endosome-associated ubiquitin isopeptidase, J. Cell Biol. 166 (2004) 487–492.
[6] M. Kyuuma, K. Kikuchi, K. Kojima, Y. Sugawara, M. Sato, N. Mano, J. Goto, T. Takeshita, A. Yamamoto, K. Sugamura, N. Tanaka, AMSH, an ESCRT-III associated enzyme, deubiquitinates cargo on MVB/late endosomes, Cell Struct. Funct. 31 (2007) 159–172.
[7] M. Agromayor, J. Martin-Serrano, Interaction of AMSH with ESCRT-III and deubiquitination of endosomal cargo, J. Biol. Chem. 281 (2006) 23083–23091.
[8] N. Ishii, Y. Owada, M. Yamada, S. Miura, K. Murata, H. Asao, H. Kondo, K. Sugamura, Loss of neurons in the hippocampus and cerebral cortex of AMSH-deficient mice, Mol. Cell. Biol. 21 (2001) 8626–8637.
[9] C.A. Ross, M.A. Poirier, Protein aggregation and neurodegenerative disease, Nat. Med. 10 (Suppl.) (2004) S10–S17.
[10] J.A. Lee, A. Beigneux, S.T. Ahmad, S.G. Young, F.B. Gao, ESCRT-III dysfunction causes autophagosome accumulation and neurodegeneration, Curr. Biol. 17 (2007) 1561–1567.
[11] G. Skibinski, N.J. Parkinson, J.M. Brown, L. Chakrabarti, S.L. Lloyd, H. Hummerich, J.E. Nielsen, J.R. Hodges, M.G. Spillantini, T. Thusgaard, S. Brandner, A. Brun, M.N. Rossor, A. Gade, P. Johannsen, S.A. Sorensen, S. Gydesen, E.M. Fisher, J. Collinge, Mutations in the endosomal ESCRTIII-complex subunit CHMP2B in frontotemporal dementia, Nat. Genet. 37 (2005) 806–808.
[12] K. Tamai, M. Toyoshima, N. Tanaka, N. Yamamoto, Y. Owada, H. Kiyonari, K. Murata, Y. Ueno, M. Ono, T. Shimosegawa, N. Yaegashi, M. Watanabe, K. Sugamura, Loss of hrs in the central nervous system causes accumulation of ubiquitinated proteins and neurodegeneration, Am. J. Pathol. 173 (2008) 1806–1817.
[13] C. Raiborg, H. Stenmark, The ESCRT machinery in endosomal sorting of ubiquitylated membrane proteins, Nature 458 (2009) 445–452.
[14] E. Miura, M. Fukaya, T. Sato, K. Sugihara, M. Asano, K. Yoshioka, M. Watanabe, Expression and distribution of JNK/SAPK-associated scaffold protein JSAP1 in developing and adult mouse brain, J. Neurochem. 97 (2006) 1431–1446.
[15] S. Nakagawa, M. Watanabe, T. Isobe, H. Kondo, Y. Inoue, Cytological compartmentalization in the staggerer cerebellum, as revealed by calbindin immunohistochemistry for Purkinje cells, J. Comp. Neurol. 395 (1998) 112–120.
[16] M.J. Clague, S. Urbe, Endocytosis: the DUB version, Trends Cell Biol. 16 (2006) 551–559.
[17] M. Filimonenko, S. Stuffers, C. Raiborg, A. Yamamoto, L. Malerod, E.M. Fisher, A. Isaacs, A. Brech, H. Stenmark, A. Simonsen, Functional multivesicular bodies are required for autophagic clearance of protein aggregates associated with neurodegenerative disease, J. Cell Biol. 179 (2007) 485–500.
[18] M. Komatsu, S. Waguri, M. Koike, Y.S. Sou, T. Ueno, T. Hara, N. Mizushima, J. Iwata, J. Ezaki, S. Murata, J. Hamazaki, Y. Nishito, S. Iemura, T. Natsume, T. Yanagawa, J. Uwayama, E. Warabi, H. Yoshida, T. Ishii, A. Kobayashi, M. Yamamoto, Z. Yue, Y. Uchiyama, E. Kominami, K. Tanaka, Homeostatic levels of p62 control cytoplasmic inclusion body formation in autophagy-deficient mice, Cell 131 (2007) 1149–1163.
[19] T.E. Rusten, A. Simonsen, ESCRT functions in autophagy and associated disease, Cell Cycle 7 (2008) 1166–1172.
[20] B. Hasdemir, J.E. Murphy, G.S. Cottrell, N.W. Bunnett, Endosomal deubiquitinating enzymes control ubiquitination and down-regulation of protease-activated receptor 2, J. Biol. Chem. 284 (2009) 28453–28466.
[21] T.M. Tzschentke, Glutamatergic mechanisms in different disease states: overview and therapeutical implications – an introduction, Amino Acids 23 (2002) 147–152.
[22] S. Pankiv, T.H. Clausen, T. Lamark, A. Brech, J.A. Bruun, H. Outzen, A. Overvatn, G. Bjorkoy, T. Johansen, P62/SQSTM1 binds directly to Atg8/LC3 to facilitate degradation of ubiquitinated protein aggregates by autophagy, J. Biol. Chem. 282 (2007) 24131–24145.
[23] F. Geser, M. Martinez-Lage, L.K. Kwong, V.M. Lee, J.Q. Trojanowski, Amyotrophic lateral sclerosis, frontotemporal dementia and beyond: the TDP-43 diseases, J. Neurol. 256 (2009) 1205–1214.
[24] N.J. Cairns, M. Neumann, E.H. Bigio, I.E. Holm, D. Troost, K.J. Hatanpaa, C. Foong, C.L. White 3rd, J.A. Schneider, H.A. Kretzschmar, D. Carter, L. Taylor-Reinwald, K. Paulsmeyer, J. Strider, M. Gitcho, A.M. Goate, J.C. Morris, M. Mishra, L.K. Kwong, A. Stieber, Y. Xu, M.S. Forman, J.Q. Trojanowski, V.M. Lee, I.R. Mackenzie, TDP-43 in familial and sporadic frontotemporal lobar degeneration with ubiquitin inclusions, Am. J. Pathol. 171 (2007) 227–240.

Please cite this article in press as: S. Suzuki et al., AMSH is required to degrade ubiquitinated proteins in the central nervous system, Biochem. Biophys. Res. Commun. (2011), doi:10.1016/j.bbrc.2011.04.065

[25] M.J. Winton, L.M. Igaz, M.M. Wong, L.K. Kwong, J.Q. Trojanowski, V.M. Lee, Disturbance of nuclear and cytoplasmic TAR DNA-binding protein (TDP-43) induces disease-like redistribution, sequestration, and aggregate formation, J. Biol. Chem. 283 (2008) 13302–13309.
[26] M. Yamada, T. Takeshita, S. Miura, K. Murata, Y. Kimura, N. Ishii, M. Nose, H. Sakagami, H. Kondo, F. Tashiro, J.I. Miyazaki, H. Sasaki, K. Sugamura, Loss of hippocampal CA3 pyramidal neurons in mice lacking STAM1, Mol. Cell. Biol. 21 (2001) 3807–3819.
[27] Y. Tanaka, N. Tanaka, Y. Saeki, K. Tanaka, M. Murakami, T. Hirano, N. Ishii, K. Sugamura, C-Cbl-dependent monoubiquitination and lysosomal degradation of gp130, Mol. Cell. Biol. 28 (2008) 4805–4818.
[28] B. McDonald, J. Martin-Serrano, No strings attached: the ESCRT machinery in viral budding and cytokinesis, J. Cell Sci. 122 (2009) 2167–2177.
[29] C. Kersaitis, G.M. Halliday, J.J. Kril, Regional and cellular pathology in frontotemporal dementia: relationship to stage of disease in cases with and without Pick bodies, Acta Neuropathol. 108 (2004) 515–523.

Please cite this article in press as: S. Suzuki et al., AMSH is required to degrade ubiquitinated proteins in the central nervous system, Biochem. Biophys. Res. Commun. (2011), doi:10.1016/j.bbrc.2011.04.065

Biochemical and Biophysical Research Communications 399 (2010) 384–390

Contents lists available at ScienceDirect

Biochemical and Biophysical Research Communications

journal homepage: www.elsevier.com/locate/ybbrc

Exosome secretion of dendritic cells is regulated by Hrs, an ESCRT-0 protein

Keiichi Tamai [a,b,d], Nobuyuki Tanaka [c,d,*], Takashi Nakano [e], Eiji Kakazu [b], Yasuteru Kondo [b], Jun Inoue [b], Masaaki Shiina [b], Koji Fukushima [b], Tomoaki Hoshino [f], Kouichi Sano [e], Yoshiyuki Ueno [b], Tooru Shimosegawa [b], Kazuo Sugamura [a,d]

[a] Department of Microbiology and Immunology, Tohoku University Graduate School of Medicine, Sendai 980-8575, Japan
[b] Department of Gastroenterology, Tohoku University Graduate School of Medicine, Sendai 980-8575, Japan
[c] Department of Cancer Science, Tohoku University Graduate School of Medicine, Sendai 980-8575, Japan
[d] Division of Immunology, Miyagi Cancer Center Research Institute, Natori, Miyagi 981-1293, Japan
[e] Department of Preventive and Social Medicine, Osaka Medical College, Takatsuki, Osaka 569-8686, Japan
[f] Division of Respirology, Neurology, and Rheumatology, Department of Medicine, Kurume University School of Medicine, 67 Asahi-machi, Kurume 830-0011, Japan

ARTICLE INFO

Article history:
Received 16 July 2010
Available online 29 July 2010

Keywords:
Dendritic cells
ESCRT
Exosomes
Hrs

ABSTRACT

Exosomes are nanovesicles derived from multivesicular bodies (MVBs) in antigen-presenting cells. The components of the ESCRT (endosomal sorting complex required for transport) pathway are critical for the formation of MVBs, however the relationship between the ESCRT pathway and the secretion of exosomes remains unclear. We here demonstrate that Hrs, an ESCRT-0 protein, is required for fascilitating the secretion of exosomes in dendritic cells (DCs). Ultrastructural analyses showed typical saucer-shaped exosomes in the culture supernatant from both the control and Hrs-depleted DCs. However, the amount of exosome secretion was significantly decreased in Hrs-depleted DCs following stimulations with ovalbumin (OVA) as well as calcium ionophore. Antigen-presentation activity was also suppressed in exsosomes purified from Hrs-depleted DCs, while no alteration in OVA degradation was seen in Hrs-depleted DCs. These data indicated that Hrs is involved in the regulation of antigen presentation activity through the exosome secretion.

1. Introduction

Exosomes are nanovesicles (60–90 nm in diameter) surrounded by a lipid bilayer. Exosomes are secreted from a variety of cells, including antigen-presenting cells (APCs), B cells, monocytes, and dendritic cells (DCs) [1], in physiological situations. They are generated as the intraluminal vesicles (ILVs) of a sorting endosome called a multivesicular body (MVB), by the inward budding of the MVB's limiting membrane. The release of exosomes into the extracellular milieu is achieved by the direct fusion of the MVB with the plasma membrane. Exosomes possess selected cargo proteins originating from the MVB membrane, including the major histocompatibility complex (MHC), costimulatory molecules, tetraspanins, adhesion molecules, and cytosolic proteins, and the biological functions of exosomes depend mainly on the types of cargo proteins they contain. For instance, APC-derived exosomes are capable of directly sensitizing naïve T cells via the MHC/peptide complex and the costimulatory molecules on their surface [2]. On the other hand, exosome like vesicles secreted from intestinal epithelial cells can induce tolerance in an antigen peptide-specific manner [3,4]. These findings suggest that exosomes carrying MHC proteins can regulate immune responses positively or negatively in vivo.

Exosomes also contain ubiquitinated proteins, suggesting that a subset of ubiquitinated cytoplasmic proteins is actively incorporated into the MVB pathway [5]. The sorting of ubiquitinated proteins on MVBs is mediated by a series of proteins involved in vacuolar protein sorting (VPS), called endosomal sorting complex required for transport (ESCRT). The first complex that binds the cargo on endosomes is ESCRT-0 (it includes Hrs [6,7] and STAM), and with the help of the ESCRTs-I, -II, and -III, the cargo accumulates on the endosomal membrane. At the end of the sorting, an AAA-type ATPase, VPS4, disrupts the ESCRT complexes, and the membrane with its accumulated cargo is invaginated into the maturing endosome to produce an intraluminal vesicle, called an MVB. Most of the ubiquitinated cargo, which includes epithelial growth factor (EGF) receptors, c-Met, and gp130, is degraded by lysosomal proteases. A deficiency of Hrs results in abnormally enlarged endosomes

Abbreviations: APC, antigen-presenting; ESCRT, endosomal sorting complex required for transport; ILV, intraluminal vesicle; MVB, multivesicular body; MHC, major histocompatibility complex; N-Rh-PE, N-(lissamine rhodamine B sulfonyl) phosphatidyl ethanolamine; OVA, ovalbumin; TEM, transmission electron microscopy; VPS, vacuolar protein sorting.

* Corresponding author at: Division of Immunology, Miyagi Cancer Center Research Institute, 47-1 Nodayama, Medeshima-Shiode, Natori, Miyagi 981-1293, Japan. Fax: +81 22 381 1168.
E-mail address: tanaka@med.tohoku.ac.jp (N. Tanaka).

0006-291X/$ - see front matter © 2010 Elsevier Inc. All rights reserved.
doi:10.1016/j.bbrc.2010.07.083

and a marked reduction in cargo sorting to the MVBs, which accumulate ligand-activated membrane-bound growth factor receptors [8]. While most of the cargo is destined for degradation, some MVBs direct their ILVs to be secreted as exosomes by direct fusion with the plasma membrane [9]. In this context, the intracellular membrane traffic system seems to play key role in the formation and release of exosomes. Previous studies suggested that at least four Rab GTPase members, Rab5, Rab11, Rab27a and Rab27b are involved in the secretion of exosomes [10–12]. Nevertheless, the precise mechanisms of the exosome pathway are still unclear.

Considering that the importance of MVB formation in exosomal pathway, as well as the presence of ubiquitinated proteins in exosomes, we suspected that Hrs might be involved in exosomal pathway. We report here that Hrs is required for secretion of exosomes in DCs.

2. Materials and Methods

2.1. Ethics Statements

This study was conducted according to the principles expressed in the Declaration of Helsinki and Fundamental Guidelines for Animal Experiments and Related Activities. The study was approved by the research committees of the Miyagi Cancer Center and Tohoku University. All the animal experiments were conducted under the approval of the Institutional Animal Care and Use Committees of Miyagi Cancer Center and Tohoku University.

2.2. Cells

DC2.4 cells (murine DC line) were maintained in RPMI medium containing 10% fetal calf serum, 2 mM L-glutamine, 1 mM sodium pyruvate, 0.1 mM non-essential amino acids, 10 mM hepes buffer, and antibiotics. We also generated primary DCs from mouse bone marrow using a standard method, as previously described [13]. To express Hrs-specific short hairpin RNA (shRNA), a retroviral vector (pSIREN-RetroQ, BD Biosciences) was generated as described previously [14]. The target sequence consisted of nucleotide residues 302–320 (5′-AGG TAA ACG TCC GTA ACA A-3′) in the human hrs cDNA. A control plasmid, pSIREN-RetroQ-Luc, targeted bp 413–434 of firefly luciferase (5′-GCA ATA GTT CAC GCT GAA AAG-3′). The retrovirus was prepared as previously described [14].

2.3. Mice

We generated a conditional knock-out of Hrs as described previously (Acc. No. CDB0476 K, Center for Developmental Biology, Kobe, Japan) [15]. To generate a dendritic-cell-specific conditional knockout of Hrs, We crossed this mouse with a LysM-cre transgenic mouse (a gift from Dr. I. Foerster) [16]. The OT-I TCR-transgenic mice were a gift from Dr. W. Heath (Walter and Eliza Hall Institute, Melbourne, Australia) and were used as the source of $CD8^+$ T cells that were specifically responsive to the OVA257–264 peptide [17].

2.4. Genotype analysis

The *hrs flox* allele was genotyped as described previously [15]. Genotyping for the presence of the LysM-Cre allele was performed using the following primer pair: forward (5′-TTA CCG GTC GAT GCA ACG AGT GAT G) and reverse (5′-TTC CAT GAG TGA ACG AAC CTG GTC G).

2.5. Isolation and purification of exosomes

Exosomes were purified as previously described [2,18]. In brief, the cell culture medium was centrifuged for 10 min at 300 g, 10 min at 1200 g, and 30 min at 10,000 g to remove the cells and debris. The supernatant obtained from the last spin was then centrifuged for 60 min at 100,000 g, and the pellet was solubilized in SDS sample buffer for analyses by Western blotting.

2.6. Fluorescent N-Rh-PE measurement

To measure exosome secretion, the fluorescent phospholipid analog N-(lissamine rhodamine B sulfonyl) phosphatidyl ethanolamine (N-Rh-PE) was inserted into the plasma membrane as described previously [19], and eventually secreted into the extracellular medium [10]. Briefly, the lipid was solubilized in absolute ethanol and injected into serum-free RPMI (<1% v/v) during vigorous vortexing. The mixture was then added to the cells, which were incubated for 60 min at 4 °C. After this incubation, the medium was removed, and the cells were extensively washed with cold PBS. The labeled cells were cultured in complete RPMI medium to collect the exosomes. To measure the exosome secretion, 50 μl of the exosomal fraction was solubilized in 1.5 ml PBS containing 0.1% Triton X-100, and the N-Rh-PE was measured at 560 nm and 590 nm excitation and emission wavelengths, respectively.

2.7. OVA protein degradation

Control and Hrs-depleted dendritic cell lines were treated with a lysosomal inhibitor (50 mM NH_4Cl) and/or proteasomal inhibitor (10 μM epoxomicin) for up to 2 h. The cells were pulsed with 300 μg/ml ovalbumin (OVA) protein for 1 h, and incubated with fresh medium for the indicated times. For western blot analysis, an anti-OVA antibody (rabbit polyclonal antibody, Abnova, Taiwan) was used for the first antibody.

2.8. Western blotting

Immunoblotting was carried out as described previously [20]. For dot-blot analysis, each cell lysate was spotted onto PVDF membranes.

2.9. Phenotypic analysis of cells by flow cytometry

Cells were assessed for surface marker expression by fluorescent multicolor flow cytometry (FACSCalibur, Becton Dickinson, San Jose, CA). The immunophenotypic profile of DCs was evaluated by staining with anti-CD40, anti-CD80, anti-I-A^β, and anti-H-2 K^β antibodies (Pharmingen).

2.10. Antigen presentation assays

To assess the function of DC-derived exosomes, we performed an in vitro $CD8^+$ T-cell proliferation assay as described previously [21]. The spleen was harvested from OT-I mice, and the $CD8^+$ T cells were positively selected using MACS magnetic beads (Miltenyi Biotec). Next, 4×10^6 BMDCs from $Hrs^{+/+}$; LysM-Cre and $Hrs^{flox/flox}$; LysM-Cre mice were incubated with 300 mg/ml OVA for 24 h. Exosomes in 10 ml of supernatant were purified as described above. The purified OT-I $CD8^+$ T cells were cocultured with the purified exosomes in 96-well plates for 5 days. The exosome induced proliferation of the OT-I T cells was measured after 5 days by adding [^{3}H]thymidine (1 μCi/well; ICN Pharmaceuticals) during the last 8 h of each culture.

2.11. Negative staining in electron microscopy

Samples of exosomes pelletted by ultracentrifugation as described above were resuspended in 0.1% glutaraldehyde, and a

drop of each resuspension was mounted on an ion-coated copper grid supported by a carbon-coated collodion film. The grid was stained with 1% uranyl acetate for 1 min and observed under an electron microscope (H-7650, Hitachi, Tokyo, Japan).

3. Results

3.1. Establishment of Hrs-depleted DCs and purification of exosomes

To examine the role of Hrs in exosome secretion, we established an Hrs-depleted dendritic cell (DC) line through retrovirus-mediated shRNA expression (Fig. 1A). The exosome-containing fractions were purified from the DCs by sucrose gradient centrifugation, using an anti-MHC-class II (I-A^{β}) antibody to detect the exosomes. The fraction containing the peak I-A^{β}-binding activity occurred at 1.15 g/ml sucrose in the sample from control DCs, and 1.14 g/ml from the Hrs-depleted DCs, indicating a similar distribution irrespective of the Hrs expression (Fig. 1B). Although these values were slightly different, they were both within the normal density profile for DC-derived exosomes in sucrose gradients [22]. Ultrastructural analysis of the ultracentrifuged exosome pellets by negative stain method of transmission electron microscopy (TEM) showed them to be markedly enriched in typical saucer-shaped exosomes, 40–100 nm in diameter, from both the control and knock-out DCs (Fig. 1C).

We further examined the exosome-containing fractions by Western blot analysis. Exosomes from the Hrs-depleted DCs under steady-state conditions contained less ubiquitinated protein than exosomes from control DCs, although the total ubiquitinated protein in the whole-cell lysates of both types of DCs was the same (Fig. 1D). MHC-I and -II, two marker proteins for DC-derived exosomes, were included at similar levels in the two exosome fractions (Fig. 1E). Although Hrs was not detected in the exosome fractions, TSG101 and VPS4B, two downstream ESCRT proteins, were clearly identified in the exosomes, and at lower amounts in the Hrs-depleted DCs. These data suggested that Hrs and another ESCRT trafficking pathway are involved in exosome secretion.

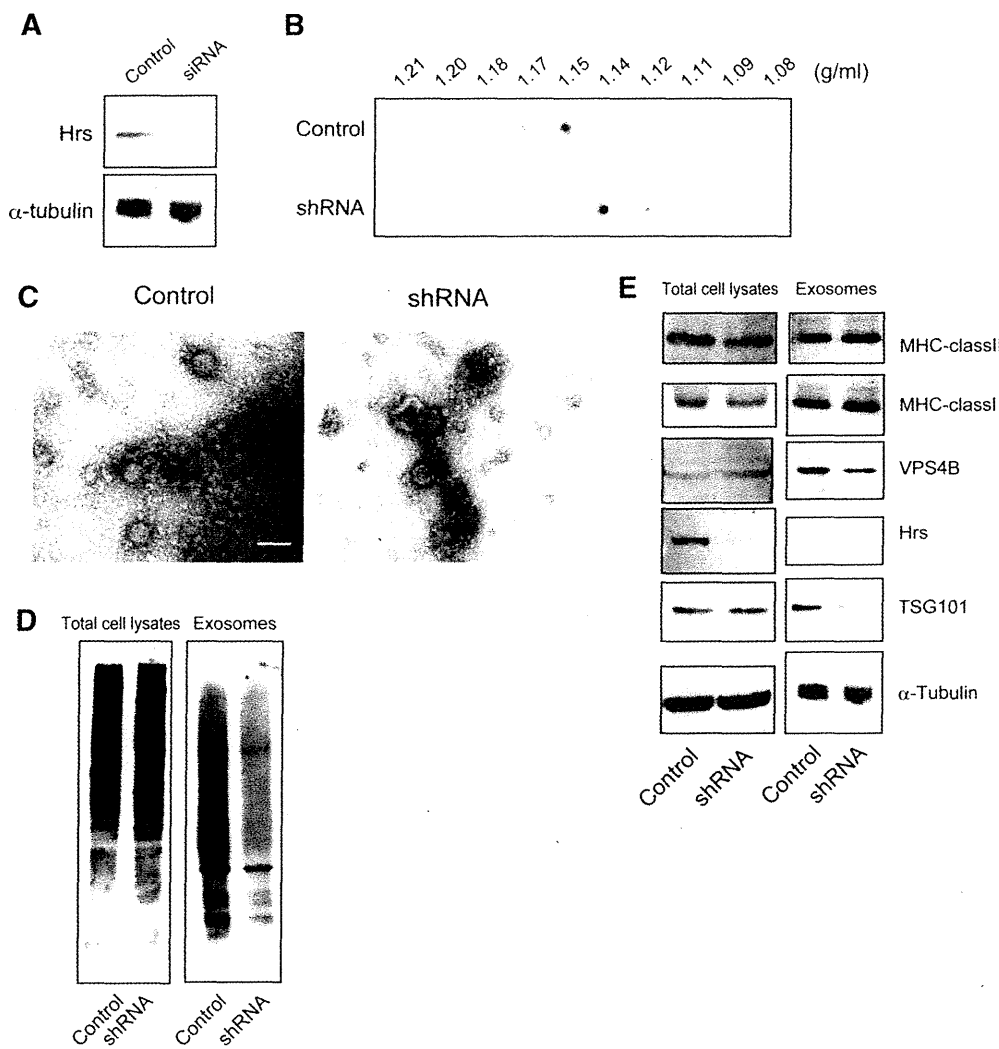

Fig. 1. Hrs-knock-down dendritic cells (DCs), Hrs knock-out bone marrow DCs, and characterization of their exosomes. (A) Western blot analysis of total cell lysates from control and Hrs knock-down DCs. (B) Sucrose gradient fractionation and dot-blot analysis of exosomes produced from DCs. The same amount of protein was fractionated and blotted on the membranes. (C) Negative staining TEM of exosomes from murine DCs. DCs were grown from monocytic precursors and cultured in GM-CSF for 10 days. The cell culture supernatants were sequentially centrifuged to obtain a pellet containing exosomes. The 100,000 x g pellet was washed and analyzed by TEM. Bar, 100 nm. (D) Western blot analysis of total cell lysates (left panel) and exosome fraction (right panel) using an antibody against ubiquitinated proteins (FK2). (E) Western blot analysis of total cell lysates (left panel) and exosomes (right panel) using the indicated antibodies.

3.2. Impairment of exosome secretion in Hrs-depleted DCs

In addition to steady-state secretion, DCs release additional exosomes upon stimulation. To examine the effect of Hrs on activation-dependent exosome secretion, the amount of purified exosomes released under several types of stimulation was measured. Ovalbumin (OVA) is known to induce exosome secretion from DCs [18,21]. Exosome secretion by the control DCs was clearly increased by 24 h of stimulation with OVA, whereas no significant increase was found in the Hrs-depleted DCs (Fig. 2A). To evaluate the possible effect of lipopolysaccharide (LPS) contamination in the OVA, we examined the amount of exosomes released under stimulation with LPS alone. Exosome secretion was not enhanced by the LPS stimulation, irrespective of the Hrs level (Fig. 2A). We also

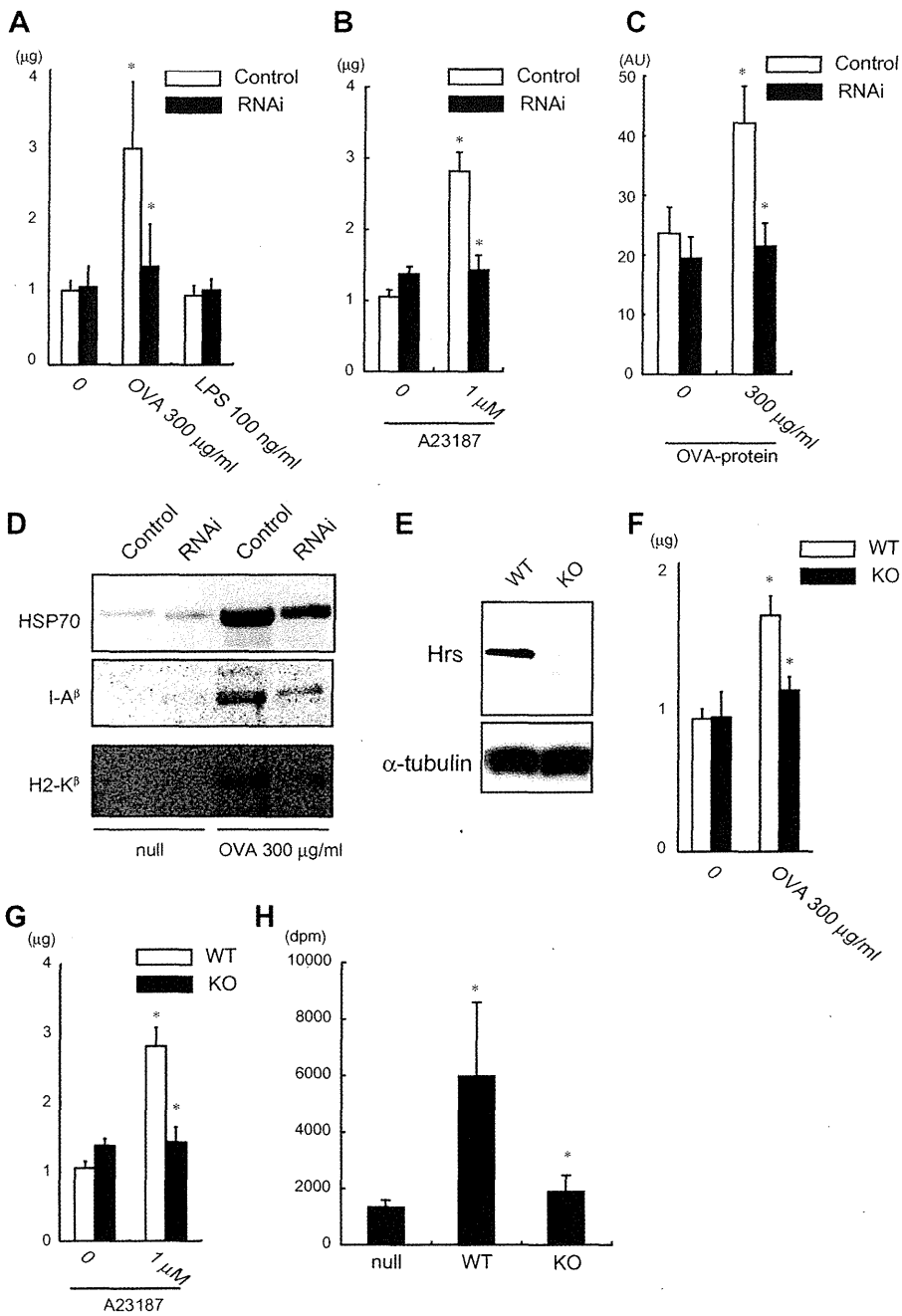

Fig. 2. Hrs is required for the secretion of exosomes. (A) Measurement of the exosome secretion from DCs under stimulation with OVA or LPS, using a protein assay. $^*p < 0.007$. (B) Measurement of exosomes under stimulation with a Ca^{2+} ionophore (1 μM A23187), using a protein assay. $^*p < 0.005$. (C) Measurement of exosome production under simulation with OVA, using N-Rh-PE release. $^*p < 0.05$. (D) Western blot analysis of exosomes under stimulation with OVA. (E) Western Blot analysis of total lysates from control and Hrs-knock out BMDCs. (F) Measurement of the exosome secretion from BMDCs under stimulation with OVA in BMDCs, using a protein assay. $^*p < 0.006$. WT, $hrs^{+/+}$, LysM-Cre; KO, $hrs^{flox/flox}$, LysM-Cre. (G) Measurement of exosomes under stimulation with a Ca^{2+} ionophore (1 μM A23187) in BMDCs, using a protein assay. $^*p < 0.005$. (H) [3H]-thymidine incorporation of CD8 T cells from OVA-specific TCR transgenic mice (OT-I mice). CD8 T cells were stimulated with purified exosomes from control and Hrs-knock out dendritic cells for 5 days. $^*p < 0.05$.

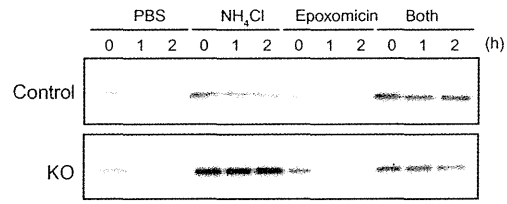

Fig. 3. Characteristics of Hrs-knock-out DCs under antigen stimulation. The degradation rate of OVA in control and Hrs-knock-down DCs was shown by western blot. A lysosomal inhibitor (NH_4Cl) and/or protease inhibitor (Epoxomicin) were included in the culture medium in some cases.

examined the exosome secretion induced by intracytoplasmic Ca^{2+} release [23]. The incubation of DCs with the Ca^{2+} ionophore A23187 induced a 2.8-fold increase in exosome release from the control DCs; however, the Hrs-depleted DCs showed very low Ca^{2+} responsiveness (Fig. 2B). We also measured the exosome secretion using N-(lissamine rhodamine B sulfonyl) phosphatidyl ethanolamine (N-Rh-PE) [10], and obtained similar results (Fig. 2C). Western blot analysis revealed that the levels of three exosome markers, HSP70, I-A^{β}, and H-2 K^{β}, were reduced in the Hrs-depleted DCs compared with the control DCs, after incubation with OVA (Fig. 2D).

To verify the essential role of Hrs in exosomal secretion, Hrs-depleted bone marrow-derived DCs (BMDCs) were successfully generated from $hrs^{flox/flox}$; LysM-Cre mice, and they expressed dramatically less Hrs than DCs derived from the $hrs^{+/+}$; LysM-Cre mice (Fig. 2E). No significant difference was seen between the population of $CD11c^{+}$ cells in BMDCs from $hrs^{+/+}$; LysM-Cre and $hrs^{flox/flox}$; LysM-Cre mice (data not shown). First, we examined the amount of exosome secretion under stimulation of OVA as well as Ca^{2+} ionophore A23187. Similar to the results obtained from Hrs-knock-down DCs, BMDCs from $hrs^{flox/flox}$; LysM-cre secreted lesser amount of exosome than those from $hrs^{+/+}$; LysM-Cre mice (Fig. 2F and G). We further investigated whether the Hrs depletion affected the amount of exosomes secreted from these cells, by measuring the antigen-presenting activity of the exosomes for T cells. DCs derived from the $hrs^{+/+}$; LysM-cre and $hrs^{flox/flox}$; LysM-Cre mice were incubated with OVA for 48 h, and the exosomes secreted from the DCs were purified. The exosomes were co-cultured with splenic $CD8^{+}$ T cells derived from OT-I transgenic mice. We found a significant increase in the proliferation of OVA-peptide restricted $CD8^{+}$ T cells cultured with the exosomes from the $hrs^{+/+}$; LysM-cre DCs, but not with those from the $hrs^{flox/flox}$; LysM-Cre DCs (Fig. 2H). Collectively, these data suggested that Hrs is required for exosome secretion.

3.3. No alteration in OVA degradation in Hrs-depleted DCs

It was possible that the decreased antigen-presentation activity of exosomes from the Hrs-depleted DCs was due to insufficient degradation of the OVA protein that was taken up. We therefore measured its degradation rate. The OVA protein was completely degraded one hour after the OVA pulse, and the degradation was the same, regardless of Hrs expression. The degradation of the OVA was efficiently blocked by a lysosomal acidification inhibitor, NH_4Cl, but not by a proteasomal inhibitor, epoxomicin, in both the control and the Hrs-depleted DCs (Fig. 3). These results suggested that Hrs does not affect the lysosome-dependent degradation of the OVA protein in DCs.

3.4. Characteristics of Hrs-depleted DCs under stimulation by OVA

We next investigated whether Hrs-depleted DCs were activated by stimulation with OVA. When stimulated with OVA proteins, DC activation markers increased more in Hrs-depleted DCs than in control cells (Fig. 4A to C). This was also true of the production of cytokines, including interleukin-6 (IL-6) and tumor necrosis factor-alpha (TNF-α) (Fig. 4D and E). These findings indicated that exosome secretion and DC activation were regulated by different mechanisms.

4. Discussion

There is accumulating evidence that the ESCRT proteins play important roles in the formation of MVBs, which undergo lysosomal digestion or are released into the extracellular environment as exosomes [24]. The ESCRT machinery, glycosylphosphatidylinositol-

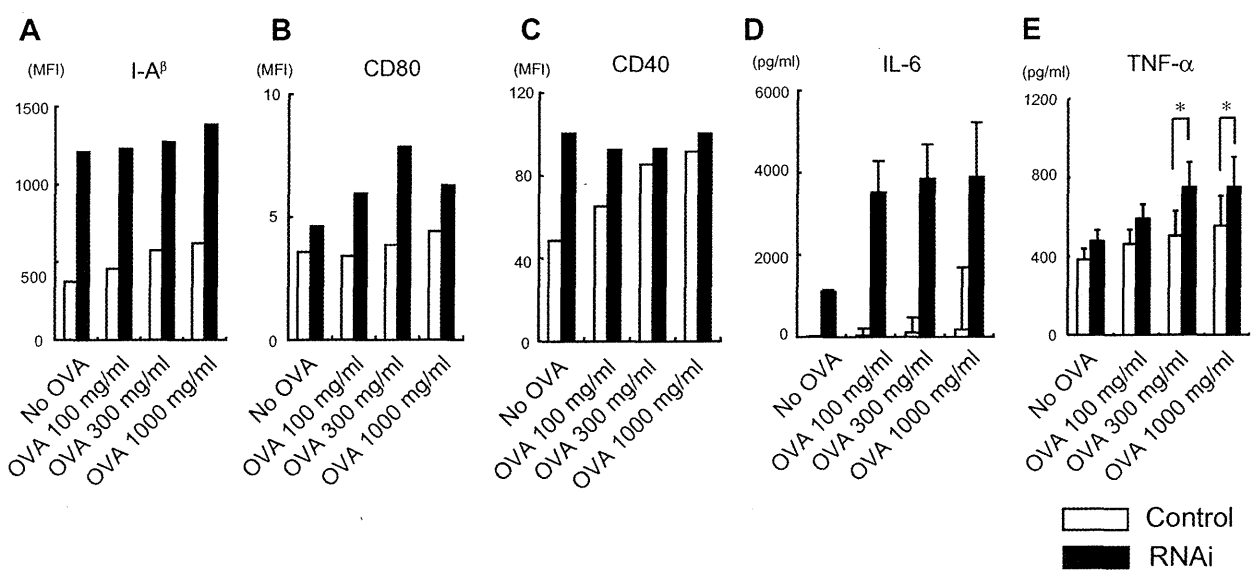

Fig. 4. Characteristics of Hrs-depleted DCs under stimulation of OVA (A to C) FACS analysis using anti-I-A^{β} (A), CD80 (B), and CD40 (C) antibodies. Control and Hrs-knock-down DCs were incubated with OVA for 24 h. Data are representative of at least three experiments. (D and E) Measurement of cytokine secretion from control and Hrs-knock-down DCs. Control and Hrs-knock-down DCs were incubated with OVA for 16 h. Data are representative of at least three experiments performed in triplicate. $^{*}p < 0.05$.

associated lipid affinity, and tetraspanin-associated protein affinity are involved in the mechanisms of cargo-protein sorting and intraluminal-vesicle formation, which are related to exosome maturation [25]. So far, two Ras family monomeric G protein Rab27a and Rab27b were reported to function in MVB docking at the plasma membrane, and to control the exosomal pathway [11], suggesting that MVBs contribute to exosome secretion through their direct fusion to the cell surface membranes. In this context, we demonstrated here that Hrs, one of the ESCRT proteins, is required for the production of exosomes within MVBs. Regarding the relationship between exosome production and the ESCRT machinery, there have been some contradictory reports. For example, the formation of proteolipid protein-containing exosomes is dependent on Rab5, but independent of the ESCRT machinery in oligodendrocytes under ceramide stimulation [12]. Since our present study on exosome production was limited to DCs stimulated by OVA or a calcium ionophore, there may be some cargo-dependent or stimulation-dependent pathways for MVB formation and exosome production.

In antigen-presenting cells, exosomes are secreted upon exposure to various stimulants, such as OVA or the calcium ionophore A23187 [18]. OVA is usually considered to act as an antigenic peptide source, and other report also utilized this agent alone to stimulate DCs [26], although we cannot fully exclude a possibility that a faint contamination of LPS as a stimulator is included in OVA. The exosome secretion in Hrs-depleted DCs was decreased in spite of their higher expression of the cell-surface-activation markers, MHC class I/II molecules as compared with the control DCs. Those markers are also known to be ubiquitinated and sequestered through MVBs [27,28]. Therefore, our findings suggested that Hrs is required for the efficient endocytosis and degradation of the MHC molecules through MVB formation as well as the exosome secretion. We previously demonstrated that the deficiency of Hrs suppresses degradation of gp130, a subunit of IL-6 receptor, in HeLa cells, which leads to a prolonged and amplified IL-6 signal [8]. Epidermal growth factor receptor (EGFR) degradation is impaired and the signaling is enhanced in Hrs-depleted mouse embryonic fibroblasts and *Drosophila* [29,30]. We suspect that Hrs-depleted DCs may be more sensitive to some stimulations than control DCs. This may be true of IL-6 secretion, because the Hrs-depleted cells secreted small but significantly more IL-6 even in the absence of OVA (Fig. 4D). It is possible that IL-6 secretion is somewhat enhanced by a factor(s) contained in FCS in the medium without OVA stimulation. We suspect that both the prolongation of cytokine signals and the deficiency of exosome production in Hrs-depleted DCs are caused by the impaired MVB formation.

Finally, our present study suggests a biological role of Hrs in immune regulation (Fig. 2H). DC-derived exosomes have been shown to have potent immunostimulatory potential, and MHC-I and B7.2 (CD86)-bearing exosomes generate $CD8^+$ T-cell responses against tumors in vivo [31]. Further study using DC-specific Hrs knockout mice will provide precise roles of the Hrs-dependent exosomal pathway in anti-tumor immune response.

Acknowledgments

The LysM-cre transgenic mice were kindly provided by Dr. Irmgard Foerster (Technical University of Munich, Munich, Germany). The authors thank Ms. Rie Ito and Yoshihiko Fujioka for technical assistance. This work was supported by JSPS and MEXT KAKENHI (21590517, 19059001, and 22790630) and a Grant-in-Aid from Ministry of Health, Labour and Welfare.

References

[1] B. Fevrier, G. Raposo, Exosomes: endosomal-derived vesicles shipping extracellular messages, Curr. Opin. Cell. Biol. 16 (2004) 415–421.
[2] G. Raposo, H.W. Nijman, W. Stoorvogel, R. Liejendekker, C.V. Harding, C.J. Melief, H.J. Geuze, B lymphocytes secrete antigen-presenting vesicles, J. Exp. Med. 183 (1996) 1161–1172.
[3] M. Karlsson, S. Lundin, U. Dahlgren, H. Kahu, I. Pettersson, E. Telemo, "Tolerosomes" are produced by intestinal epithelial cells, Eur. J. Immunol. 31 (2001) 2892–2900.
[4] S. Ostman, M. Taube, E. Telemo, Tolerosome-induced oral tolerance is MHC dependent, Immunology 116 (2005) 464–476.
[5] S.I. Buschow, J.M. Liefhebber, R. Wubbolts, W. Stoorvogel, Exosomes contain ubiquitinated proteins, Blood Cells Mol. Dis. 35 (2005) 398–403.
[6] H. Asao, Y. Sasaki, T. Arita, N. Tanaka, K. Endo, H. Kasai, T. Takeshita, Y. Endo, T. Fujita, K. Sugamura, Hrs is associated with STAM, a signal-transducing adaptor molecule. Its suppressive effect on cytokine-induced cell growth, J. Biol. Chem. 272 (1997) 32785–32791.
[7] M. Komada, N. Kitamura, Growth factor-induced tyrosine phosphorylation of Hrs, a novel 115-kilodalton protein with a structurally conserved putative zinc finger domain, Mol. Cell. Biol. 15 (1995) 6213–6221.
[8] Y. Tanaka, N. Tanaka, Y. Saeki, K. Tanaka, M. Murakami, T. Hirano, N. Ishii, K. Sugamura, c-Cbl-dependent monoubiquitination and lysosomal degradation of gp130, Mol. Cell Biol. 28 (2008) 4805–4818.
[9] S.I. Buschow, E.N. Nolte-'t Hoen, G. van Niel, M.S. Pols, T. ten Broeke, M. Lauwen, F. Ossendorp, C.J. Melief, G. Raposo, R. Wubbolts, M.H. Wauben, W. Stoorvogel, MHC II in dendritic cells is targeted to lysosomes or T cell-induced exosomes via distinct multivesicular body pathways, Traffic 10 (2009) 1528–1542.
[10] A. Savina, M. Vidal, M.I. Colombo, The exosome pathway in K562 cells is regulated by Rab11, J. Cell Sci. 115 (2002) 2505–2515.
[11] M. Ostrowski, N.B. Carmo, S. Krumeich, I. Fanget, G. Raposo, A. Savina, C.F. Moita, K. Schauer, A.N. Hume, R.P. Freitas, B. Goud, P. Benaroch, N. Hacohen, M. Fukuda, C. Desnos, M.C. Seabra, F. Darchen, S. Amigorena, L.F. Moita, C. Thery, Rab27a and Rab27b control different steps of the exosome secretion pathway, Nat. Cell Biol. 12 (2010) 19–30. sup pp 11-13.
[12] K. Trajkovic, C. Hsu, S. Chiantia, L. Rajendran, D. Wenzel, F. Wieland, P. Schwille, B. Brugger, M. Simons, Ceramide triggers budding of exosome vesicles into multivesicular endosomes, Science 319 (2008) 1244–1247.
[13] M.B. Lutz, N. Kukutsch, A.L. Ogilvie, S. Rossner, F. Koch, N. Romani, G. Schuler, An advanced culture method for generating large quantities of highly pure dendritic cells from mouse bone marrow, J. Immunol. Methods 223 (1999) 77–92.
[14] K. Tamai, N. Tanaka, A. Nara, A. Yamamoto, I. Nakagawa, T. Yoshimori, Y. Ueno, T. Shimosegawa, K. Sugamura, Role of Hrs in maturation of autophagosomes in mammalian cells, Biochem. Biophys. Res. Commun. 360 (2007) 721–727.
[15] K. Tamai, M. Toyoshima, N. Tanaka, N. Yamamoto, Y. Owada, H. Kiyonari, K. Murata, Y. Ueno, M. Ono, T. Shimosegawa, N. Yaegashi, M. Watanabe, K. Sugamura, Loss of hrs in the central nervous system causes accumulation of ubiquitinated proteins and neurodegeneration, Am. J. Pathol. 173 (2008) 1806–1817.
[16] B.E. Clausen, C. Burkhardt, W. Reith, R. Renkawitz, I. Forster, Conditional gene targeting in macrophages and granulocytes using LysMcre mice, Transgenic Res. 8 (1999) 265–277.
[17] S.R. Clarke, M. Barnden, C. Kurts, F.R. Carbone, J.F. Miller, W.R. Heath, Characterization of the ovalbumin-specific TCR transgenic line OT-I: MHC elements for positive and negative selection, Immunol. Cell. Biol. 78 (2000) 110–117.
[18] S. Hao, O. Bai, J. Yuan, M. Qureshi, J. Xiang, Dendritic cell-derived exosomes stimulate stronger $CD8^+$ CTL responses and antitumor immunity than tumor cell-derived exosomes, Cell. Mol. Immunol. 3 (2006) 205–211.
[19] J. Willem, M. ter Beest, G. Scherphof, D. Hoekstra, A non-exchangeable fluorescent phospholipid analog as a membrane traffic marker of the endocytic pathway, Eur. J. Cell. Biol. 53 (1990) 173–184.
[20] N. Tanaka, K. Kaneko, H. Asao, H. Kasai, Y. Endo, T. Fujita, T. Takeshita, K. Sugamura, Possible involvement of a novel STAM-associated molecule "AMSH" in intracellular signal transduction mediated by cytokines, J. Biol. Chem. 274 (1999) 19129–19135.
[21] S. Hao, O. Bai, F. Li, J. Yuan, S. Laferte, J. Xiang, Mature dendritic cells pulsed with exosomes stimulate efficient cytotoxic T-lymphocyte responses and antitumour immunity, Immunology 120 (2007) 90–102.
[22] C. Thery, A. Regnault, J. Garin, J. Wolfers, L. Zitvogel, P. Ricciardi-Castagnoli, G. Raposo, S. Amigorena, Molecular characterization of dendritic cell-derived exosomes. Selective accumulation of the heat shock protein hsc73, J. Cell Biol. 147 (1999) 599–610.
[23] A. Savina, C.M. Fader, M.T. Damiani, M.I. Colombo, Rab11 promotes docking and fusion of multivesicular bodies in a calcium-dependent manner, Traffic 6 (2005) 131–143.
[24] A. de Gassart, C. Geminard, D. Hoekstra, M. Vidal, Exosome secretion: the art of reutilizing nonrecycled proteins?, Traffic 5 (2004) 896–903
[25] G. van Niel, I. Porto-Carreiro, S. Simoes, G. Raposo, Exosomes: a common pathway for a specialized function, J. Biochem. 140 (2006) 13–21.
[26] K. Akiyama, S. Ebihara, A. Yada, K. Matsumura, S. Aiba, T. Nukiwa, T. Takai, Targeting apoptotic tumor cells to Fc gamma R provides efficient and versatile vaccination against tumors by dendritic cells, J. Immunol. 170 (2003) 1641–1648.

[27] L.M. Duncan, S. Piper, R.B. Dodd, M.K. Saville, C.M. Sanderson, J.P. Luzio, P.J. Lehner, Lysine-63-linked ubiquitination is required for endolysosomal degradation of class I molecules, EMBO. J. 25 (2006) 1635–1645.
[28] J.S. Shin, M. Ebersold, M. Pypaert, L. Delamarre, A. Hartley, I. Mellman, Surface expression of MHC class II in dendritic cells is controlled by regulated ubiquitination, Nature 444 (2006) 115–118.
[29] T.E. Lloyd, R. Atkinson, M.N. Wu, Y. Zhou, G. Pennetta, H.J. Bellen, Hrs regulates endosome membrane invagination and tyrosine kinase receptor signaling in Drosophila, Cell 108 (2002) 261–269.
[30] C. Kanazawa, E. Morita, M. Yamada, N. Ishii, S. Miura, H. Asao, T. Yoshimori, K. Sugamura, Effects of deficiencies of STAMs and Hrs, mammalian class E Vps proteins, on receptor downregulation, Biochem. Biophys. Res. Commun. 309 (2003) 848–856.
[31] L. Zitvogel, A. Regnault, A. Lozier, J. Wolfers, C. Flament, D. Tenza, P. Ricciardi-Castagnoli, G. Raposo, S. Amigorena, Eradication of established murine tumors using a novel cell-free vaccine: dendritic cell-derived exosomes, Nat. Med. 4 (1998) 594–600.